SIGNAL ENHANCEMENT OF SURFACE SCATTERED UNDERWATER SOUND

Maurice Anthony Tourville

NAVAL POSTGRADUATE SCHOOL
Monterey, California

THESIS

SIGNAL ENHANCEMENT OF
SURFACE SCATTERED UNDERWATER SOUND

by

Maurice Anthony Tourville III

June 1975

Thesis Advisor: H. Medwin

REPORT DOCUMENTATION PAGE

READ INSTRUCTIONS BEFORE COMPLETING FORM

1. REPORT NUMBER
2. GOVT ACCESSION NO.
3. RECIPIENT'S CATALOG NUMBER

4. TITLE (and Subtitle)
Signal Enhancement of Surface Scattered Underwater Sound

5. TYPE OF REPORT & PERIOD COVERED
Master's Thesis; June 1975

6. PERFORMING ORG. REPORT NUMBER

7. AUTHOR(s)
Maurice Anthony Tourville III

8. CONTRACT OR GRANT NUMBER(s)

9. PERFORMING ORGANIZATION NAME AND ADDRESS
Naval Postgraduate School
Monterey, California 93940

10. PROGRAM ELEMENT, PROJECT, TASK AREA & WORK UNIT NUMBERS

11. CONTROLLING OFFICE NAME AND ADDRESS
Naval Postgraduate School
Monterey, California 93940

12. REPORT DATE
June 1975

13. NUMBER OF PAGES
100

14. MONITORING AGENCY NAME & ADDRESS(if different from Controlling Office)

15. SECURITY CLASS. (of this report)
UNCLASSIFIED

15a. DECLASSIFICATION/DOWNGRADING SCHEDULE

16. DISTRIBUTION STATEMENT (of this Report)
Approved for public release; distribution unlimited.

17. DISTRIBUTION STATEMENT (of the abstract entered in Block 20, if different from Report)

18. SUPPLEMENTARY NOTES

19. KEY WORDS (Continue on reverse side if necessary and identify by block number)
Phase-shift processing
Acoustic signal processing
Scattered sound
Lloyd Mirror Effect

20. ABSTRACT (Continue on reverse side if necessary and identify by block number)

The wind-driven surface of a large anechoic tank was used to study scattered underwater sound. Twenty kilohertz CW signals were transmitted by an omnidirectional source. Two directional receivers, mounted together, were oriented to individually monitor the direct and surface-reflected signals. Several methods of signal addition by means of digital FFT analysis were used to increase average received power and

(20. ABSTRACT Continued)

reduce temporal fluctuations in the output. The most promising technique, when compared to the case of an omni-directional receiver, increased the average signal power by as much as 12 dB, while reducing the coefficient of power variation by as much as 50%. The amount of improvement depends on the size and location of the receiver with respect to the surface interference pattern, and the acoustical roughness of the surface, g. Roughnesses in this experiment were approximately g = 0.7 and 1.5, where $g = 4k^2\sigma^2\cos^2\theta$ and k is the wave number, σ is the rms surface wave height, and θ the angle of incidence and reflection.

Signal Enhancement of Surface Scattered Underwater Sound

by

Maurice Anthony Tourville III
Ensign, United States Navy
B.S.E.E., Ohio State University, 1974

Submitted in partial fulfillment of the
requirements for the degree of

MASTER OF SCIENCE IN ENGINEERING ACOUSTICS

from the

NAVAL POSTGRADUATE SCHOOL
June 1975

ABSTRACT

The wind-driven surface of a large anechoic tank was used to study scattered underwater sound. Twenty kilohertz CW signals were transmitted by an omnidirectional source. Two directional receivers, mounted together, were oriented to individually monitor the direct and surface-reflected signals. Several methods of signal addition by means of digital FFT analysis were used to increase average received power and reduce temporal fluctuations in the output. The most promising technique, when compared to the case of an omnidirectional receiver, increased the average signal power by as much as 12 db, while reducing the coefficient of power variation by as much as 50%. The amount of improvement depends on the size and location of the receiver with respect to the surface interference pattern, and the acoustical roughness of the surface, g. Roughnesses in this experiment were approximately $g = 0.7$ and 1.5, where $g = 4k^2\sigma^2\cos^2\theta$ and k is the wave number, σ is the rms surface wave height, and θ the angle of incidence and reflection.

TABLE OF CONTENTS

LIST OF FIGURES

ACKNOWLEDGMENT

The author wishes to express his sincere appreciation to the following for assistance during this research:

Dr. Herman Medwin provided a seemingly endless source of support and guidance. Of particular note was his ability to patiently consider, constructively criticize, and practically apply new ideas.

Mr. William Smith was always ready with new solutions to the typical problems that arise during the course of laboratory work. His practical experience and technical expertise saved countless hours of labor.

Mrs. Carol Hickey made possible all digital processing in this research. Her ability to correctly interpret the description of a physical problem and to convert its proposed solution into computer programs was excellent.

Pinkerton Computer Consultants Inc., through Mr. Tom Lee and Mr. Les Stevens, of Interdata Corporation, aided in the maintainance of the OPHELEA system.

The Manager and Staff of the ASW Systems Project Office, ASW-12, have maintained continuing interest and support for this research.

I. INTRODUCTION

When an acoustic signal travels through the ocean, many things can happen to it. Marine life, ocean boundaries, and the inhomogeneous nature of the medium can affect the propagation of sound. A number of variable factors, such as depth, salinity and temperature will combine to produce a sound speed that varies with position. Thus, an acoustic signal received at one location in the ocean may be drastically different from the signal originally emitted by a distant source.

In particular, if a constant amplitude, constant frequency signal is generated, propagated, or received near the ocean surface, the amplitude of the signal is known to rise and fall as time passes. This fluctuating signal is usually monitored in either of two ways; by the human observer using an audio version of the signal, or by electronic systems designed to extract certain characteristics from the signal. Each method has advantages and disadvantages. The human ear is superior in that it can automatically tune out certain frequencies and amplitudes in order to receive only those of interest. In addition, the ear has the advantage of selective integration -- that is, whether he is conscious of it or not, the observer listens when the signal is loud, and tunes out when the signal falls. This is an extreme advantage over the

continuous integration found in electronic signal processing systems. These systems cannot selectively process in time. All signals, including those that have faded, are averaged together. The results of the averaging process will reflect this fact. However, electronic systems have great merits. Their response time and amplitude and frequency resolution capabilities are far superior to any human.

A. OBJECTIVE

The objective of this research is to propose and investigate new signal monitoring techniques that combine the advantages and/or eliminate the disadvantages mentioned above. To pursue this objective, the cause of acoustic fluctuations in this work will be the time varying ocean surface. Any other ocean phenomenon that may cause underwater acoustic signals to fluctuate has not been considered in this research.

B. INTERMEDIATE GOALS

The following intermediate goals are presented as stepping stones towards the objective of this research:

i) develop laboratory modeling techniques that allow accurate simulation of various real world ocean surfaces

ii) verify that the ocean model affects acoustic waves as theory predicts and as actual ocean measurements show

iii) investigate signal processing possibilities to decrease, minimize, and/or eliminate the cancellation effects of the ocean surface on acoustic waves

II. SURVEY OF FORMAL THEORETICAL APPROACHES

The scattering of wave energy from uneven surfaces is a problem that has been quite popular over the past twenty to twenty-five years. Increased interest in both electromagnetic and acoustic wave scattering has resulted in many recent articles in the literature.[1] Numerous authors, utilizing various mathematical methods, have attempted to describe the scattered fields resulting from a wide range of boundaries. Simply stated, the task is to solve the wave equation with boundary conditions that are determined by the scattering surface. This is not always easy, and, in fact, is usually accomplished only after severe restrictions and/or sometimes doubtful assumptions have been introduced.

A. LIMITATIONS

The assumptions that appear in theoretical studies of scattering are almost as numerous as the studies themselves. In terms of underwater sound scattered from a time varying, random ocean surface, many of these assumptions strictly

---

[1] Both acoustic and electromagnetic wave studies give rise to the same mathematics. The usual distinction lies in the fact that the wavelengths typical of electromagnetic radiation used for sensing (e.g. radar, light) are usually much smaller than the boundary dimensions, and ray theory or geometrical optics can be used as a simple approach. In acoustics, the wavelength of the radiation is often on the order of the boundary dimensions, and a diffraction theory is called for.

limit mathematical predictions of resultant acoustic fields. Some of the common assumptions, such as a constant amplitude, constant frequency source, and a fixed source/receiver geometry are tolerable. (This situation can be realized easily and accurately in the lab and at sea.) Other theoretical restrictions, however, may be quite severe.

Early work in the subject of scattering concentrated on fixed periodic surfaces. At the end of the nineteenth century, Lord Rayleigh proposed a solution for scattering from a fixed sinusoidal surface [Ref. 1]. (His solution has been expanded and criticized by a number of authors. Some examples can be found in Refs. 2, 3, and 4.) Works on fixed, random surfaces can also be found in the literature [Refs. 5,6]. Usually, an equation describing the height, slope, frequency spectrum, probability density function, or correlation function of the random surface is assumed. The limitations in this area are obvious. The ocean surface is not only random in spatial coordinates, it is also time varying. The need for descriptions of the random ocean surface in both space and time introduces extreme complications.

Even if the above mentioned solutions for fixed random surfaces could be generalized to include time dependences, other factors would cause complications. Theoretical work to date assumes the medium to be homogeneous and to possess a static, non-turbulent, bubble free subsurface layer. Again, in terms of real ocean acoustics, this is highly unlikely.

Several well known solutions make use of the Helmholtz integral. This technique requires some information about the pressure field and/or its normal derivatives on the boundary (the ocean surface). The surface is usually assumed to be a perfect pressure release surface, and the pressure on the boundary is thus set to zero. Difficulties can arise in specifying the normal derivative of the pressure on the surface. (In fact, simply specifying the direction of the normal to the surface at every point can be a problem.) The common assumption made here is the familiar 'Kirchhoff approximation' which holds only for locally flat surfaces. (Simply stated, this approximation uses on a point to point basis, the reflection coefficient for a plane wave incident on an infinitely large, flat surface.) A systematic derivation and a quantitative discussion of the limits of its validity are given by Meecham in Ref. 7.

One restriction that appears frequently has to do with the so-called roughness parameter,

$$(g)^{\frac{1}{2}} = (2\pi\sigma/\lambda)\ (\cos\theta_1 + \cos\theta_2)$$

This parameter is a measure of the acoustical roughness in terms of the wavelength (λ) of the acoustical energy, the angles of incidence and reflection (θ_1, θ_2), and the rms height of the surface (σ). Most analyses deal with situations where the roughness parameter is either small or large

compared to unity. For small roughness parameters, the amplitude of the scattered sound possesses a Gaussian probability density function. As the roughness parameter increases beyond 1, the statistics gradually shift from Gaussian to Rayleigh. Selecting low or high values of g with respect to 1 allows either a Gaussian or Rayleigh probability density function to be used to statistically describe the scattered sound. Low or high values of g also may simplify the problem by minimizing complications that arise due to shadowing and/or diffraction. Multiple scattering is also a very real possibility, and is usually neglected in scattering problems.

At one point or another, most theoretical attempts have a statement that begins, 'a constant amplitude, constant frequency plane wave is incident on a surface described by ...' . As previously mentioned, the monochromatic restrictions are not too severe. However, the plane wave assumption, an assumption that is almost universally made, should not be carelessly bypassed. Wavefront curvature does occur, introducing both sound phase and amplitude changes away from the beam axis of the source. Although this is not always important, the critical reader should be aware of subtle implications hidden in the plane wave assumption.

A comprehensive textbook by Beckmann and Spizzichino [Ref. 8], which studies the theoretical scattering of electromagnetic waves, is quite applicable to the problem of

acoustic scattering. Notable, in depth surveys of theoretical scattering problems with extensive bibliographies have been published by two authors. Lysanov [Ref. 9] surveys the area up to 1958, and includes 79 references, while Fortuin [Ref. 10] gives an updated survey to 1969 with 87 references. Both articles are excellent reviews of the subject. This author's feelings towards strict theoretical solutions to the scattering problem are best described by Fortuin: "A large number of publications in the open literature are devoted to the subject. But they all cover only part of the problem: all of them are restricted to a special case, and are based on certain assumptions – sometimes rather arbitrary – that make simplifications possible but at the same time cast doubt on their validity." [Ref. 10, p. 1210]

B. SUMMARY

1. Experiment as a Supplement to Theory

The above comments concerning the pitfalls of strictly theoretical approaches to the scattering problem have been made in order that the need for supplemental experimental research be noted. The true acoustical engineer is not only concerned with complex mathematical expressions, his interest lies also in improving man's ability to control energy in its acoustic form. A careful mixture of theoretical insight and controlled experimental procedure is sometimes more fruitful than purely theoretical studies with unacceptable

or unworkable assumptions. Such is the philosophy adopted for this research.

2. The Engineering Approach

The author has begun by posing for himself the following question: "If a monochromatic point source

$$p_s = A \cos \omega t$$

generates waves that are in some way affected by the ocean surface, how does a point receiver interpret the incoming energy?"

In words, the answer is simple — the tone rises and falls. This is the commonly known amplitude modulation. Closer scrutiny reveals that the received signal also has a time varying phase shift with respect to the source. Hence, the received signal can be written as

$$p_r = \{A + B(t)\} \cos \{\omega t + \phi(t)\}$$

The problem as the acoustical engineer now sees it is to predict, eliminate, and/or compensate for the amplitude and phase fluctuations in the received signal so that the final version of the received signal more closely resembles the signal sent out by the source.

III. RESEARCH FACILITIES

The first goal of this research, as given in Section I.B, is to 'develop laboratory modeling techniques that allow accurate simulation of various real world ocean surfaces'. The Ocean Acoustic Wave Facility at the Naval Postgraduate School is an established laboratory model that has been designed to meet these requirements. (Verification of the fact that the model accurately simulates the real ocean will be given later in Section IV.A.) A description of the Ocean Acoustic Wave Facility (hereafter called the OAWF), its associated laboratory, and data gathering capabilities is now presented.

A. OAWF

The OAWF is a unique combination of a wind generated water wave tunnel and an anechoic acoustic tank. Water waves are generated by 1 to 5 centrifugal fans. The 3/4 horsepower fans are arranged so that they blow over a water surface in a tunnel. The tunnel is approximately 17 meters long, 1.2 meters wide, and 1.2 meters deep. By varying the number of fans and/or the distance between the water surface and the top of the tunnel, a wide range of ocean surfaces can be simulated. Observation windows are located at various points along the tunnel allowing the growth of the waves to be observed (see Figure 1).

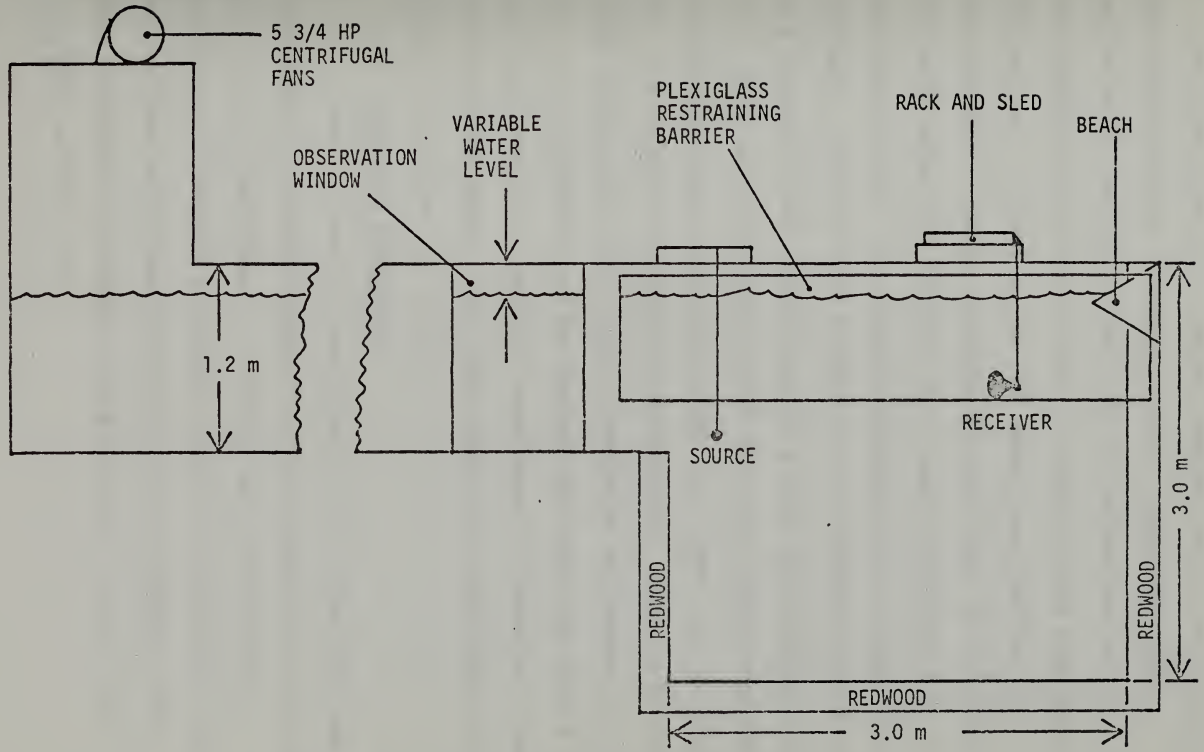

Figure 1. Side View of OAWF

The wave generation tunnel empties into a water filled tank approximately 3 meters square. Since the waves generated in the tunnel are only 1.2 meters across, a plexiglass restraining barrier is used to keep them from diffracting over the entire 3x3 meter tank surface area (see Figure 2). Upon reaching the back wall of the tank, the water waves are absorbed by a beach constructed in a triangular shape from aluminum shavings and a nylon mesh. The tank itself is made anechoic on the bottom and all sides by a lining of 4x4 redwood posts, placed with corners facing out. (The tank wall along which the water waves pass has the redwood beams positioned with flat sides out, in order that the waves will pass by undisturbed.) The use of redwood beams ensures excellent sound absorption as pointed out in Ref. 11. Equipment can be lowered into the tank with a position accuracy of about 1 centimeter by means of a movable rack and sled setup. The OAWF models the real ocean on a scale of the order of 50 to 1.

1. Standard Equipment

Most of the equipment used in the generation and reception of acoustic signals in this research was standard, off the shelf equipment. In order to avoid continual reference to lengthy equipment titles, the following lists full titles and/or descriptions of the equipment, along with corresponding abbreviations that will be used for the remainder of the text:

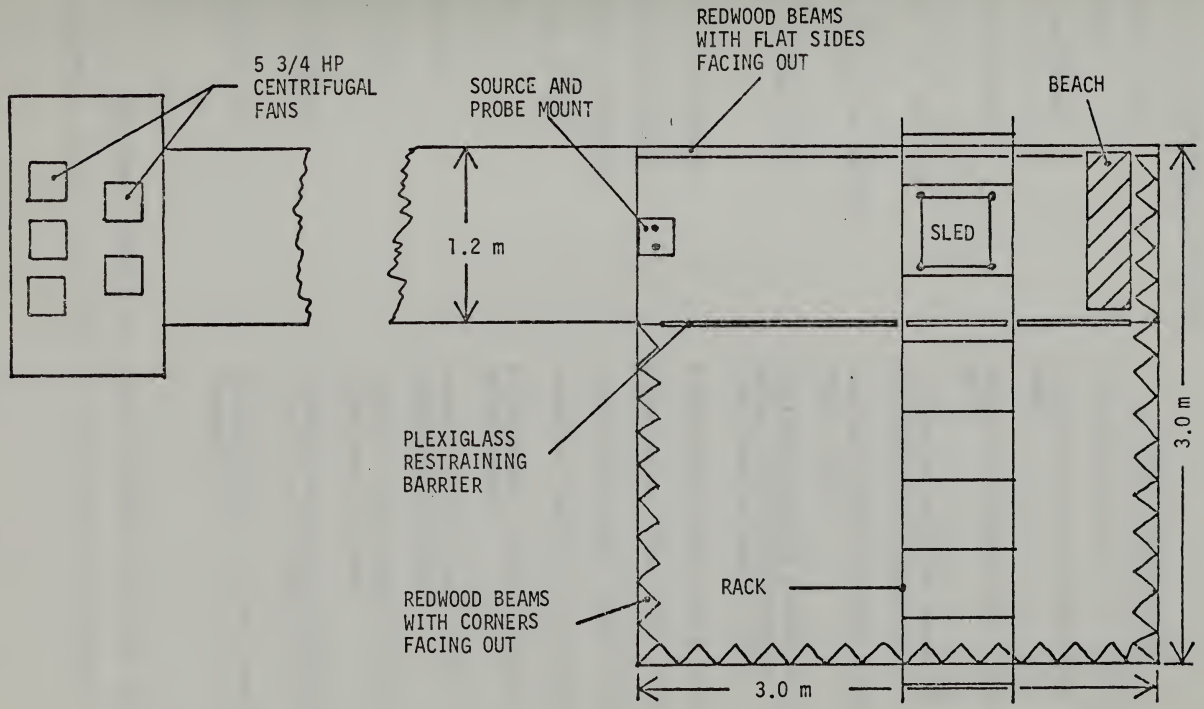

Figure 2. Top View of OAWF

LIST OF STANDARD EQUIPMENT

Abbreviation	Full Description
Scope	Tektronix Model 545B Oscilloscope
HP 466A AMP	Hewlett-Packard Amplifier Model 466A
HP 467A AMP	Hewlett-Packard Amplifier Model 467A
PAR 113 PRE-AMP	Princeton Applied Research Preamplifier Model 113
HP 721A PWR SUPPLY	Hewlett-Packard Power Supply Model 721A
HP 3300A/3302A	Hewlett-Packard Function Generator, Model 3300A with Trigger/Phase Lock Module Model 3302A
KH 3322 FILTER	Krohn-Hite Model 3322 Filter
KH 3342 FILTER	Krohn-Hite Model 3342 Filter
KH 3350 FILTER	Krohn-Hite Model 3350 Filter
FREQ METER	Monsanto Model 100A Counter-Timer
DMM	Fluke Model 8000A Digital Multi-Meter
GR 1312	General Radio Model 1312 Decade Oscillator
Z-Bridge	General Radio Model 1650A Impedance Bridge
PHASE METER	Dranetz Series 305 Phase Meter with Plug-in Module 305-PA-30001
WAVTEK 144	Wavtek Model 144 HF Sweep/Signal Generator

Sources, receivers, wave probes, and other such equipment will be described in the text as necessary.

2. Data Acquisition and Processing Capabilities

Data acquisition and processing in this research was accomplished by utilizing a system nicknamed OPHELEA, an acronym for Ocean Physics Environmental Effects Analyzer. The system has three major components: 1) a pair of Phoenix Analog to Digital Converters, Model ADC 712 2) an INTERDATA Model 70 Computer 3) a Texas Instruments Silent 700 Electronic Data Terminal, Model 733. System design and interfacing was developed by the Special Projects Section of the Naval Air Development Center in conjunction with Pinkerton Computer Consultants of Warminster, Pennsylvania. The system is shown in Figure 3.

The Phoenix A/D converters are high speed devices capable of converting analog voltages in the ± 10 volt range into 12 bits (11 bits plus sign) of digital information. This results in an accuracy of 1 part in 4095, or 5 millivolts in 20 volts. The converter has performed reliably at rates as high as 400,000 conversions per second. The A/D converter requires a command to convert signal which is a positive going 5 volt pulse with a duration of at least 200 nanoseconds. This command to convert signal, hereafter called the sampling frequency, is supplied by the Wavtek 144.

The INTERDATA Model 70 computer is a 16 bit half word computer with a 32k memory. In addition to the actual core memory, data that have been previously stored on digital cassettes can be read into the computer. Due to computer

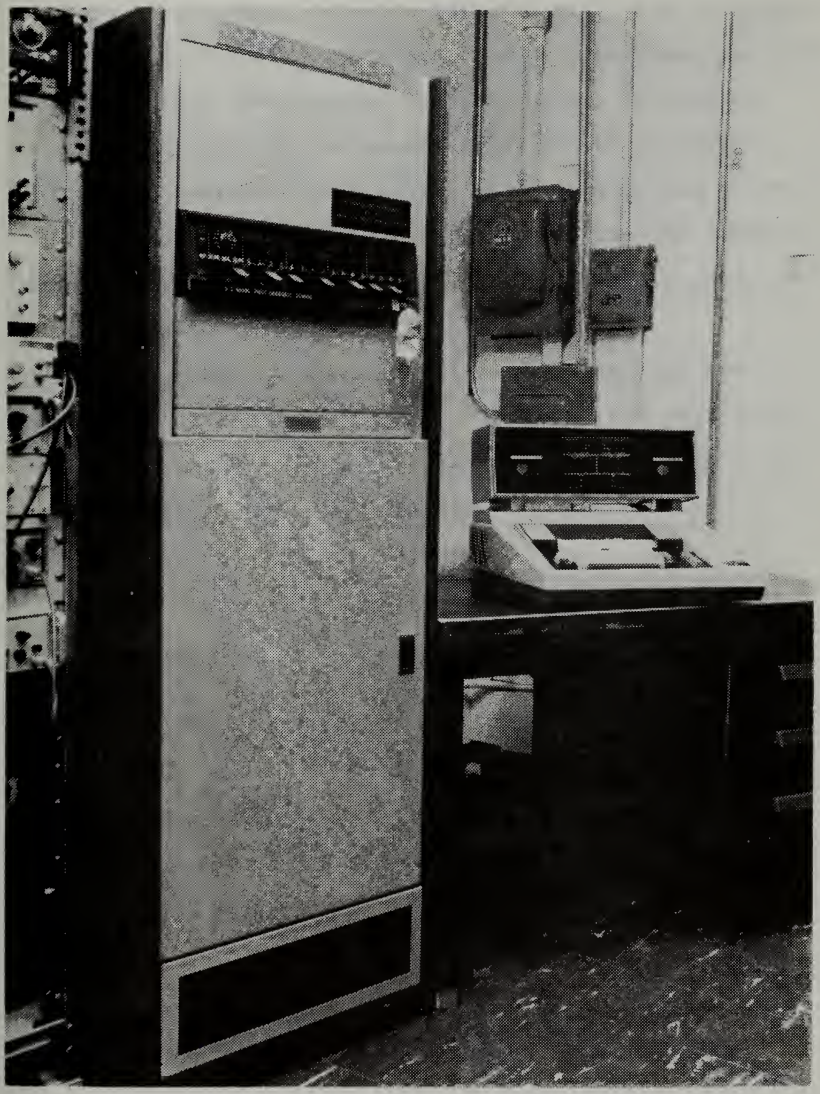

Figure 3. The OPHELEA System with Computer and A/D Converter in the Large Cabinet to the Left

storage limitations, data for this research were sometimes gathered in digital format, recorded on cassettes, and later re-loaded into the computer for processing. The Texas Instruments terminal has capabilities for this type of read/write operation in addition to a keyboard and printer that are used to communicate with and program the computer. Output appears in printed form on heat sensitive paper at the terminal output.

The OPHELEA system facilitates rapid, accurate processing of laboratory data. The system was used mainly in this research for statistical and frequency domain (by means of FFT algorithms) analysis.

IV. EXPERIMENTAL PROCEDURE AND RESULTS

This portion of the text describes attempts to reach each of the intermediate goals listed in Section I.B. Each goal is separately considered under an individual subtitle. The experimental procedures, along with the reasoning behind them, and the results, are included in each section. (Part V of this report will analyze to what degree each of the intermediate goals has been attained, and will sum the results in a discussion considering the accomplishment of the objective of this research.)

A. CONFIRMING THE ACCURACY OF THE MODEL OCEAN

The first intermediate goal of this research, as given in Section I.B, is repeated here for convenience:

> i) develop laboratory modeling techniques that allow accurate simulation of real world ocean surfaces

The OAWF, as described in Section III.A, has been designed with this goal in mind. However, this research would not be complete without verification that the waves generated in the OAWF do indeed simulate waves found at sea.

In a recent work by Perkins [Ref. 12], the wave height probability density function, frequency spectrum, and autocorrelation function of waves generated in the OAWF were studied. Perkins investigated a model ocean generated by 3 fans blowing through the wave tunnel. The distance

between the still water surface and the top of the tunnel was set to 14.25 cm. (Hereafter, this distance will be referred to as the still water level, or SWL.) Perkins found the probability density function of the wave height to be approximated by a Gaussian distribution, which is in agreement with Kinsman [Ref. 12, p. 345]. (See Figure 4.) The autocorrelation function was found to be similar to a damped cosine function, also in agreement with Kinsman. (See Figure 5.) However, for some unknown reason, the wave height frequency spectra reported by Perkins took on an odd bi-modal shape. (See Figure 6.) The following describes the steps taken in this research to use the flexibility of the OAWF to create a model ocean with a wave height frequency spectra closer to the ideal type found in the real ocean when a simple wind driven gravity wave system exists without swell.

All investigations of the wave height in this research were carried out using a highly linear, capacitive type wave probe developed by the Civil Engineering Department of Stanford University. The probe circuitry appears in block diagram form in Figure 7. The probe is connected directly to the input of a GR1650A Impedance Bridge. The bridge is usually used to measure an unknown impedance by adjusting the bridge circuitry until a balance is obtained. Here, however, the balance is adjusted with the probe in still

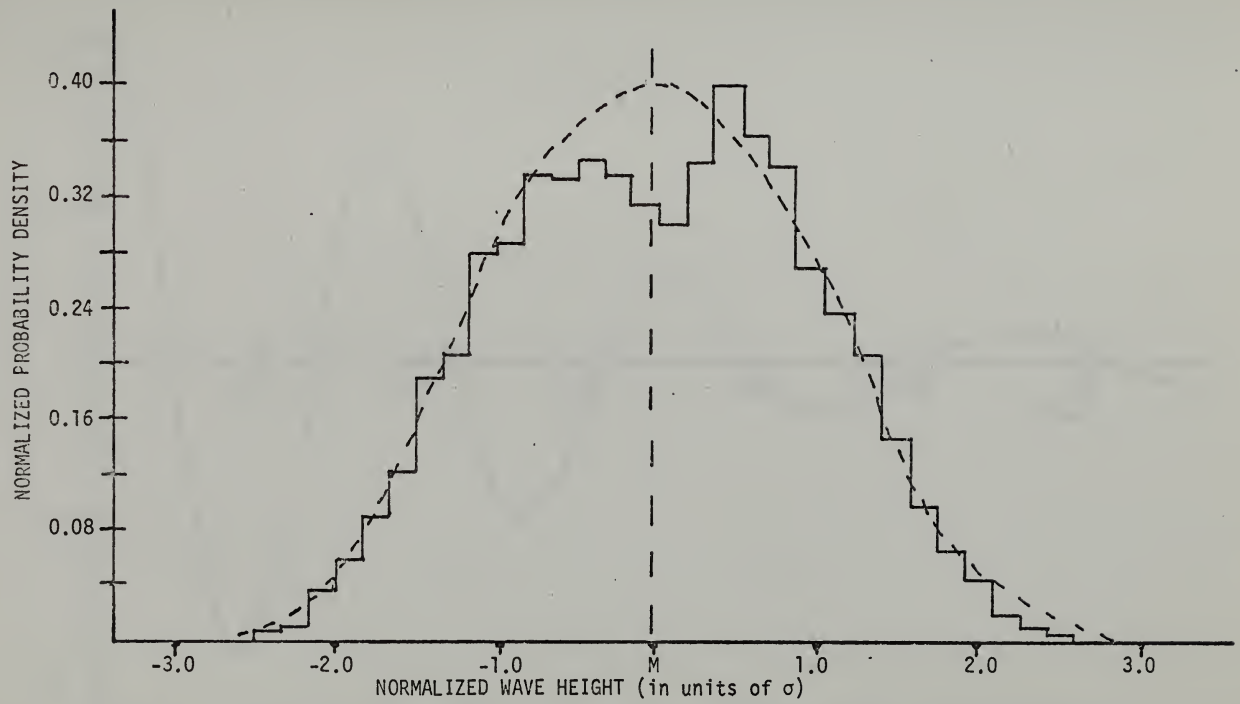

Figure 4. Wave Height Histogram and Normalized Gaussian PDF (from Perkins)

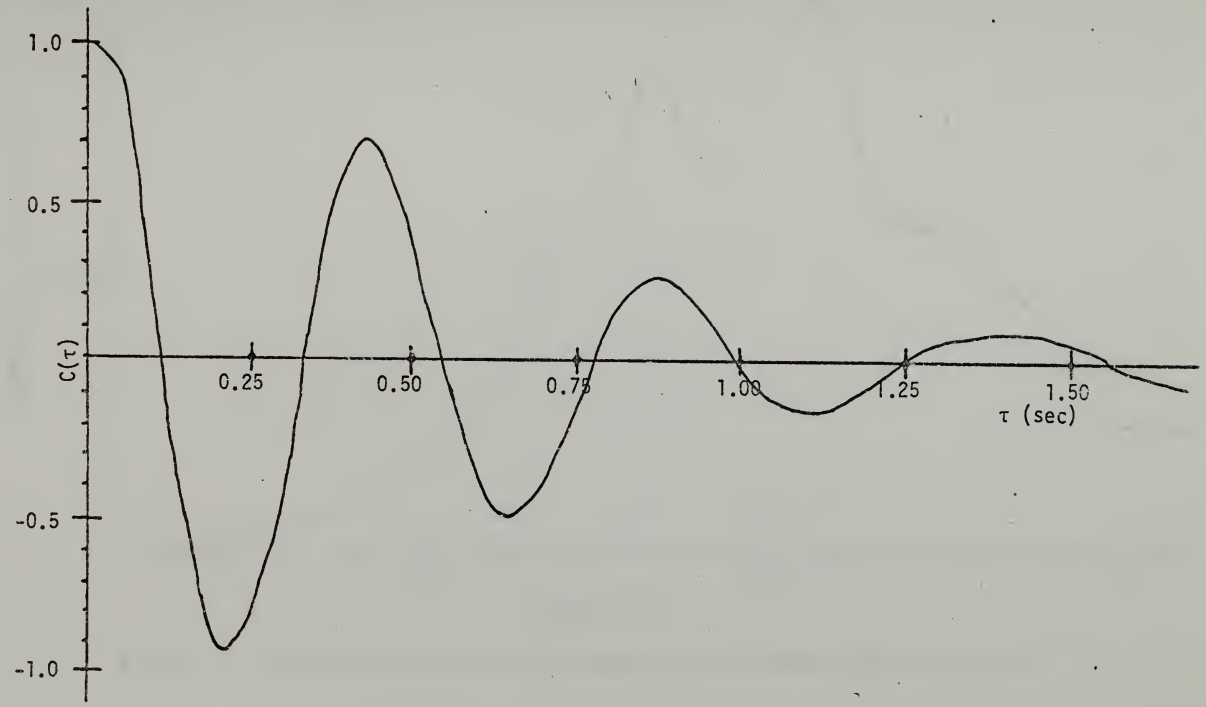

Figure 5. Average OAWF Surface Wave Height Autocorrelation Function (from Perkins)

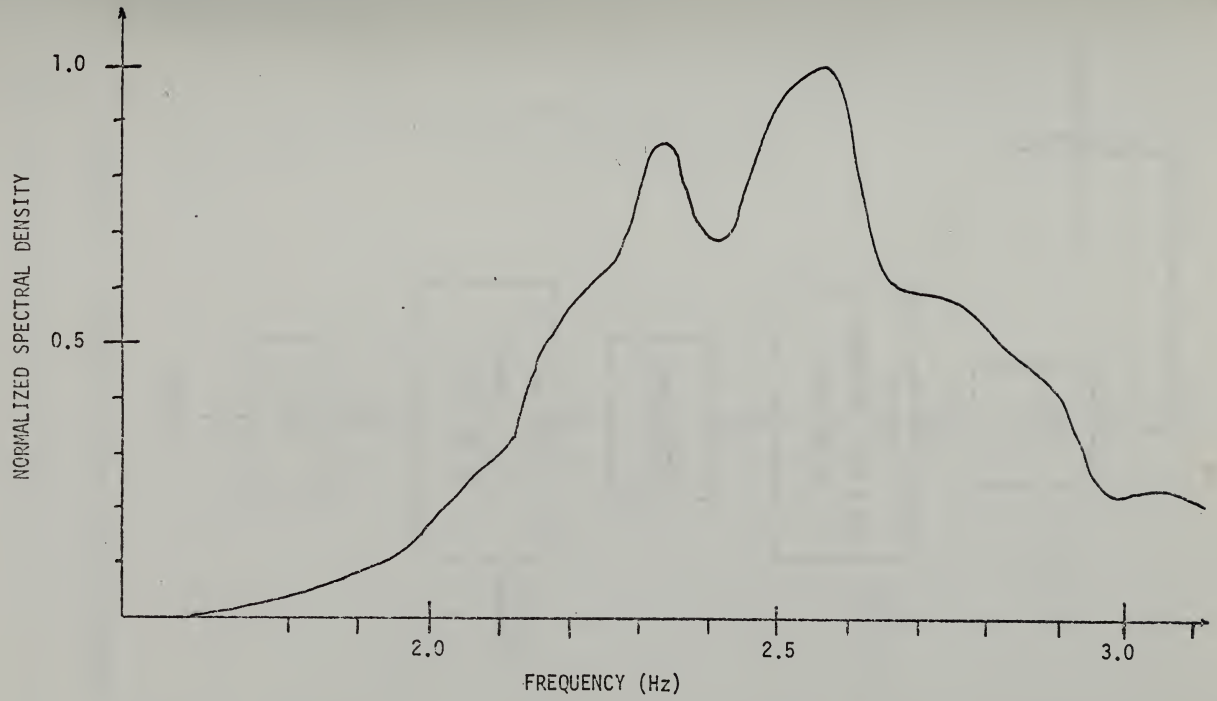

Figure 6. Normalized Wave Height Frequency Spectrum (from Perkins)

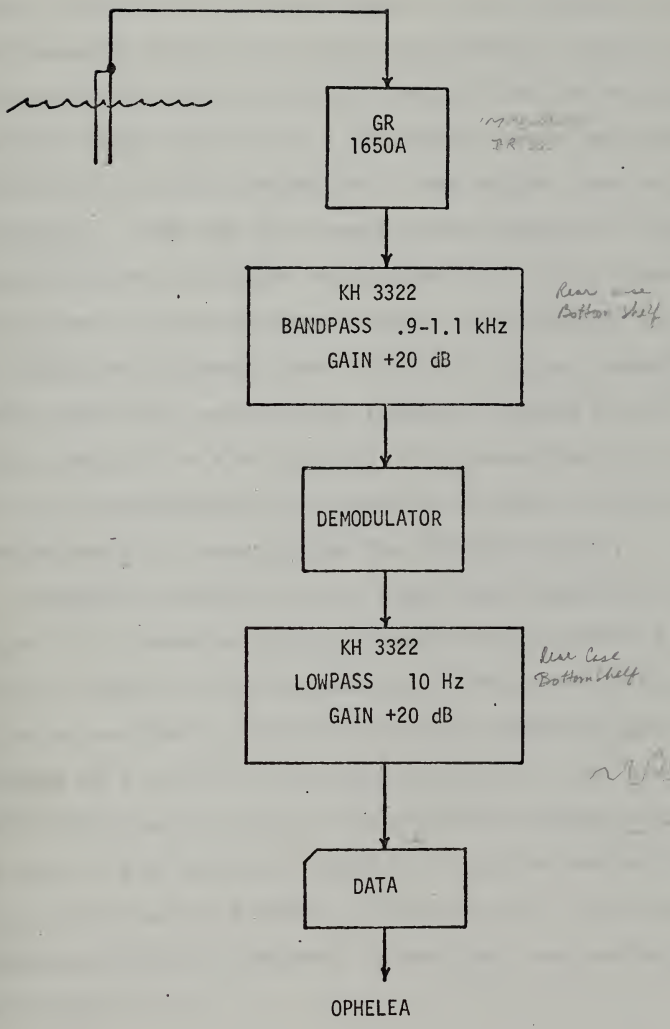

Figure 7. Capacitive Wave Probe Circuitry

water. When the fans are turned on, the varying wave height continuously changes the probe capacitance, and thus the bridge is no longer balanced. The GR1650A has an output terminal which delivers a 1 kHz signal whose amplitude is proportional to the deviation of the bridge from its balanced condition. Thus the time varying wave height at the probe appears as the amplitude modulation of a 1 kHz sinusoid at the output of the impedance bridge. This signal is amplified and bandpass filtered from .9 kHz to 1.1 kHz, demodulated, again amplified, and finally lowpass filtered at 10 Hz. The final result is a time varying dc voltage that is a replica of the instantaneous wave height at a point. This voltage is now suitable for analysis by the OPHELEA system.

Frequency analysis of the ocean wave height was done by means of a flexible computer program built around a Fast Fourier Transform (FFT) algorithm.[1] The program was designed to calculate both individual spectral densities and the average of a number of spectral densities. The number of data points to be taken for an individual spectral density, as well as the sampling frequency, could be varied to control the resolution and bandpass of the output. Up to 60 spectral densities could be computed, normalized, and averaged during one computer run.

---

[1]Copies of all computer programs used in this research have been placed on file and are available from Professor H. Medwin at the Naval Postgraduate School.

Using the OPHELEA system and the wave probe arrangement, wave height spectral densities for various model oceans were investigated. Different models were created by utilizing various fan and still water level combinations. From the numerous model ocean surfaces investigated, two were selected for use in this research. It was found that setting the still water level at 17.8 cm and using either 2 or 5 fans produced ocean models that displayed suitable spectral density functions. These two oceans, hereafter referred to as the 2 fan ocean and the 5 fan ocean, are now described.

The normalized spectral densities for the 2 fan and 5 fan oceans are shown in Figure 8. Each curve is the result of 5 data runs, each run being an average of 50 FFTs. Individual data runs processed a total of 12,800 data points, or 256 points for each of the 50 FFTs in that data run. The sampling frequency was varied slightly in each data run, in order to seek out spectral density components at different frequencies. (The minimum sampling frequency was restricted to 13 Hz to ensure fulfillment of the Nyquist criterion for the desired frequency range.) Both spectra are quite similar to the "typical spectrum of wind generated waves at short fetches" shown both experimentally and theoretically by Kinsman [Ref. 12, p. 581]. According to Kinsman, "The abrupt rise to a peak followed by a more or less smooth -5-power descent for the saturated high frequency

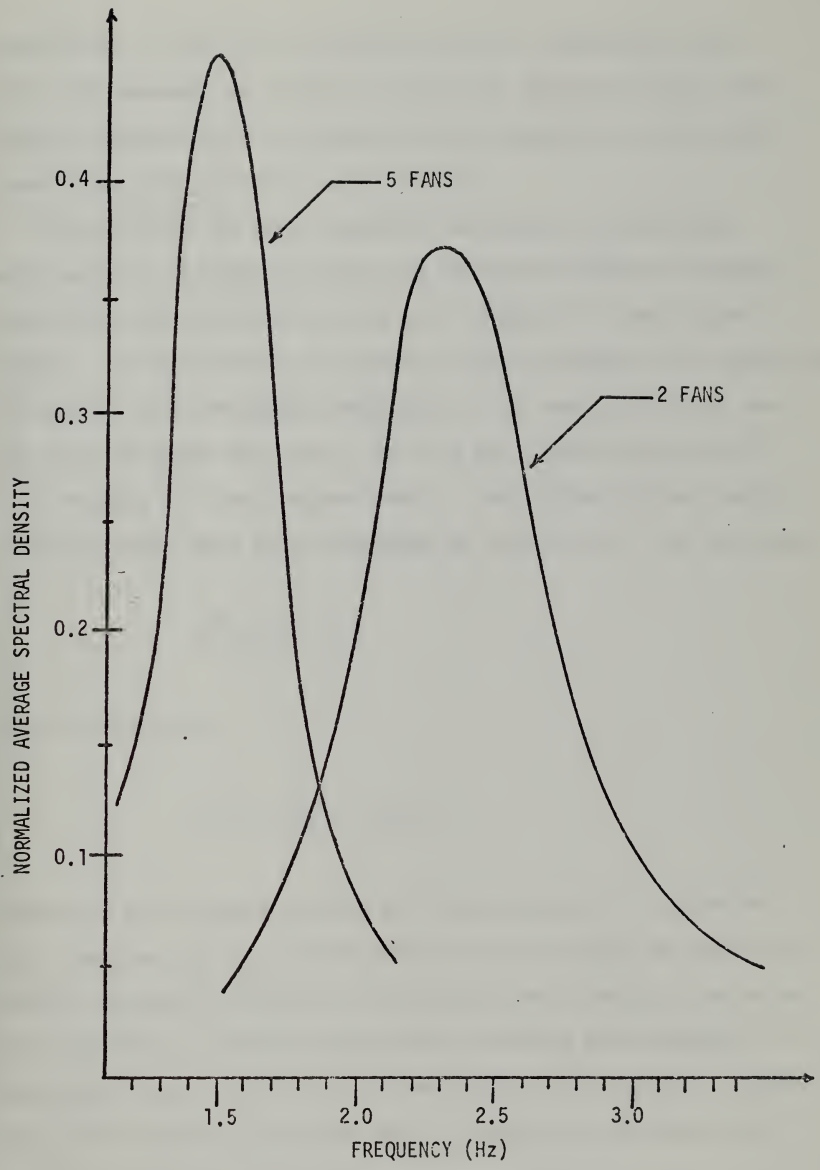

Figure 8. OAWF Wave Height Frequency Spectra

components is entirely characteristic." Comparison with this f-5 descent is shown in Figure 9, where the high frequency components of the wave height spectra of both model oceans are plotted on a log-log grid.

In addition to the frequency analysis of the ocean wave height, a short statistical analysis computer program was used to determine the rms wave height for both ocean models. As previously discussed, this information is required to specify the roughness parameter. It was found that the rms wave heights for the 2 fan and the 5 fan oceans were 0.75 cm and 1.10 cm respectively. The higher order statistical moments were also computed at this time. The skewness

$$\langle h^3 \rangle / 2 \langle h^2 \rangle^{3/2}$$

and the kurtosis

$$(\langle h^4 \rangle - 3 \langle h^2 \rangle^2) / 2 \langle h^2 \rangle^2$$

(where h is the wave height and the brackets <> indicate the average) are an indication of the deviation of the wave height probability density function from a perfect Gaussian distribution. The variations for the OAWF are somewhat stronger than those found in the typical Kinsman sea. However, the values are comparable as shown by the following table:

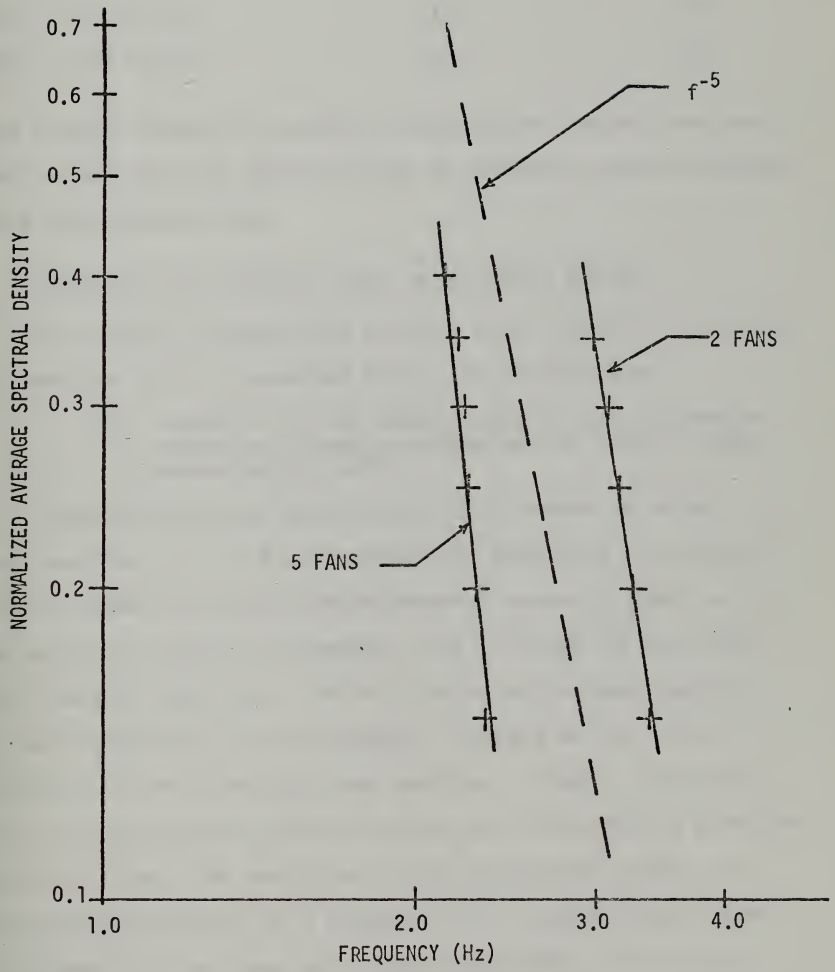

Figure 9. OAWF Wave Height Frequency Spectra Compared with f^{-5} Dependence

	Skewness	Kurtosis
Kinsman-record 072	.092	- .031
OAWF 2 Fan Ocean	.167	- .437
OAWF 5 Fan Ocean	.103	- .321

The higher values of kurtosis (peakedness) in the OAWF are due to the greater contributions of capillary waves compared to a pure gravity sea.

B. EFFECTS OF THE MODEL OCEAN ON ACOUSTIC WAVES

The second intermediate goal of this research, as given in Section I.B, is repeated here, for convenience:

> ii) verify that the model ocean affects acoustic waves as theory predicts and as actual ocean measurements show

This verification can be made in a number of ways. Parkins [Ref. 13] has mathematically predicted the effects of the ocean surface on monochromatic acoustic plane waves in terms of several parameters, one of which is the ocean wave height spectrum. The derivation by Parkins results in an expression for the spectral density of the sound scattered from a moving ocean surface. Simply summarized, for a monochromatic acoustic plane wave incident on a moving ocean surface, the spectrum of the reradiated signal is frequency modulated by a Doppler shift term and amplitude modulated by the ocean wave height spectrum. It is the amplitude modulation term that is of interest here.

The surface of the model ocean has been shown to accurately simulate a scaled down version of the real ocean. If a CW signal scattered from waves generated in the OAWF possesses an amplitude modulation whose frequency spectrum is similar to the frequency spectrum of the wave height, then the ocean model, at least by this criterion, affects acoustic waves as predicted by the theory of Parkins'. The following experiment was conducted to investigate this phenomenon.[1]

In the OAWF, an omnidirectional source was placed at a depth of 20 cm, and an omnidirectional receiver at a depth of 30 cm was located downrange 128 cm. The source was constructed by coating a 2" (o.d.) Glennite Ceramic sphere with several coats of neopreme. A GR 1312 Decade Oscillator was used to drive the source. (Hereafter, this source will be referred to as OMNI.) A standard Atlantic Research LC-10 hydrophone was used as the receiver. The LC-10 was immediately amplified by a 30 db NUS Corporation FET preamp powered by 12 volts dc supplied by an HP 721A power supply. This signal was then amplified, demodulated, and lowpass filtered. The experimental setup is shown in block diagram form in Figure 10.

---

[1]The assumptions used by Parkins should be noted here. The ocean surface is assumed to be generated by a stationary, homogeneous, Gaussian process, and is assumed to be smooth enough so that shadowing and multiple scattering can be neglected. Plane waves, an isovelocity medium, and a perfect pressure release surface are also assumed. Of course, results are given only for the cases of the slightly rough surface and the very rough surface. It is obvious from these facts that the comparison of Parkins theory with the following experimental results will be semi-quantitative in nature.

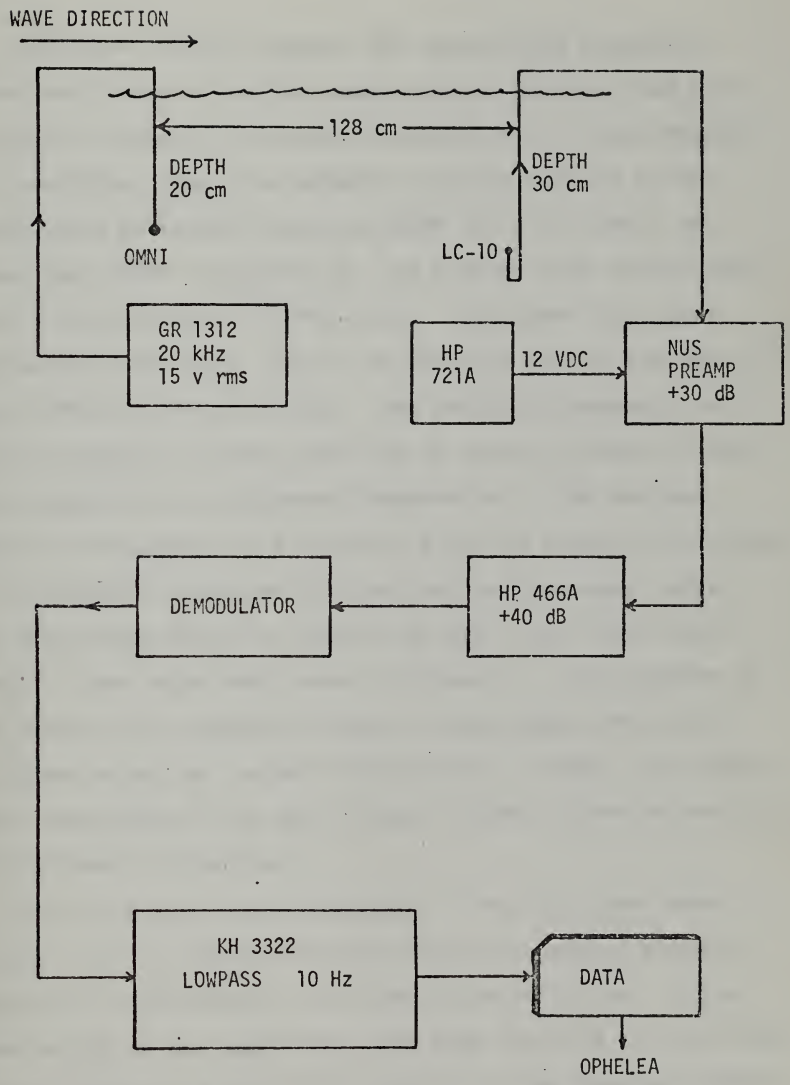

Figure 10. Experimental Setup for Investigating Demodulated Scattered Sound

Using the OPHELEA system, the demodulated scattered sound was processed by the same computer program used previously to compute the spectral density of the wave height. The resulting normalized average spectral density of the demodulated scattered sound for both the 2 fan and 5 fan oceans are shown in Figure 11. As before, each curve represents 5 data runs of 50 FFTs each. Individual data runs processed 12,800 data points, or 256 data points for each of the 50 FFTs in that data run. The sampling frequency was varied slightly for each data run in order to seek out spectral components at different frequencies. (The minimum sampling frequency was limited to 13 Hz to ensure fulfillment of the Nyquist criterion for the desired frequency range.) For easy comparison, the curves for the ocean wave height spectrum have also been shown in Figure 11. The spectra of the demodulated scattered sound and the ocean wave height do indeed match up for both ocean models. Hence, the water waves generated in the OAWF affect acoustic waves as predicted by the theory of Parkins.

At this point in the research, it was felt that some insight into the nature of the fluctuating signal might be gained by investigating its phase characteristics. Close observation of the amplitude modulated sinusoid at the output reveals that the signal also displays a time dependent phase shift. That is, the received signal is of the form

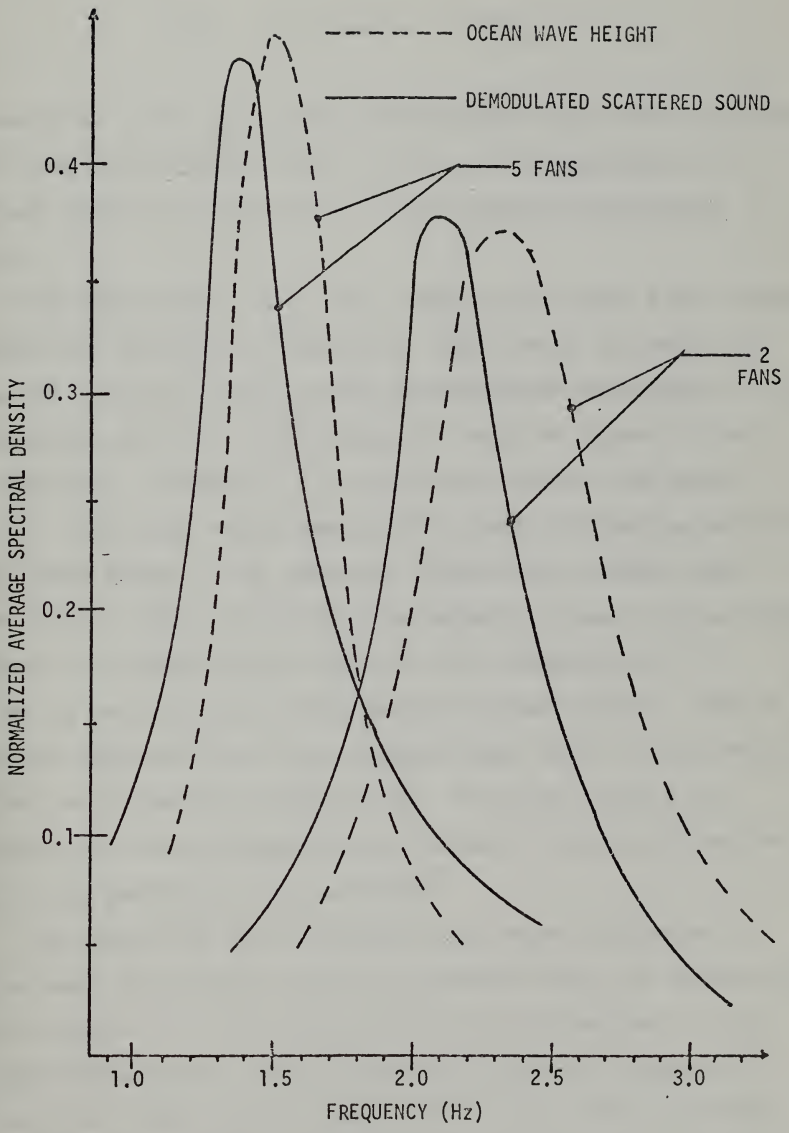

Figure 11. Comparison of Spectral Densities of Demodulated Scattered Sound and Ocean Wave Height

$$v(t) = A(t) \cos\{\omega t + \phi(t)\}$$

where A(t) is the previously investigated amplitude modulation. The time varying phase shift, $\phi(t)$, was investigated in a manner similar to that used for the amplitude modulation term.

The experimental setup for investigating this time varying phase term is shown in Figure 12. This setup is similar to the one used for investigating the amplitude modulation. The difference is that in this case the received signal is not demodulated. Instead, it is fed into a Dranetz 305 phase meter. The phase meter measures the phase difference between two input signals; the reference signal was obtained from the GR1312, which was driving the source. Along with a digital readout, the phase meter puts out a dc voltage which is directly proportional to the amount of phase shift. This dc voltage represents the time varying phase shift of the received signal with respect to the source. The time varying dc voltage was then processed by the OPHELEA system just as the amplitude modulation was processed.

The results of this experiment are shown in Figure 13. (The ocean wave height spectra are shown also, for comparison.) These curves represent the average spectral density of the phase fluctuations. They indicate that phase fluctuations occur over times that are comparable to the times characteristic of the amplitude fluctuations, but they do not match

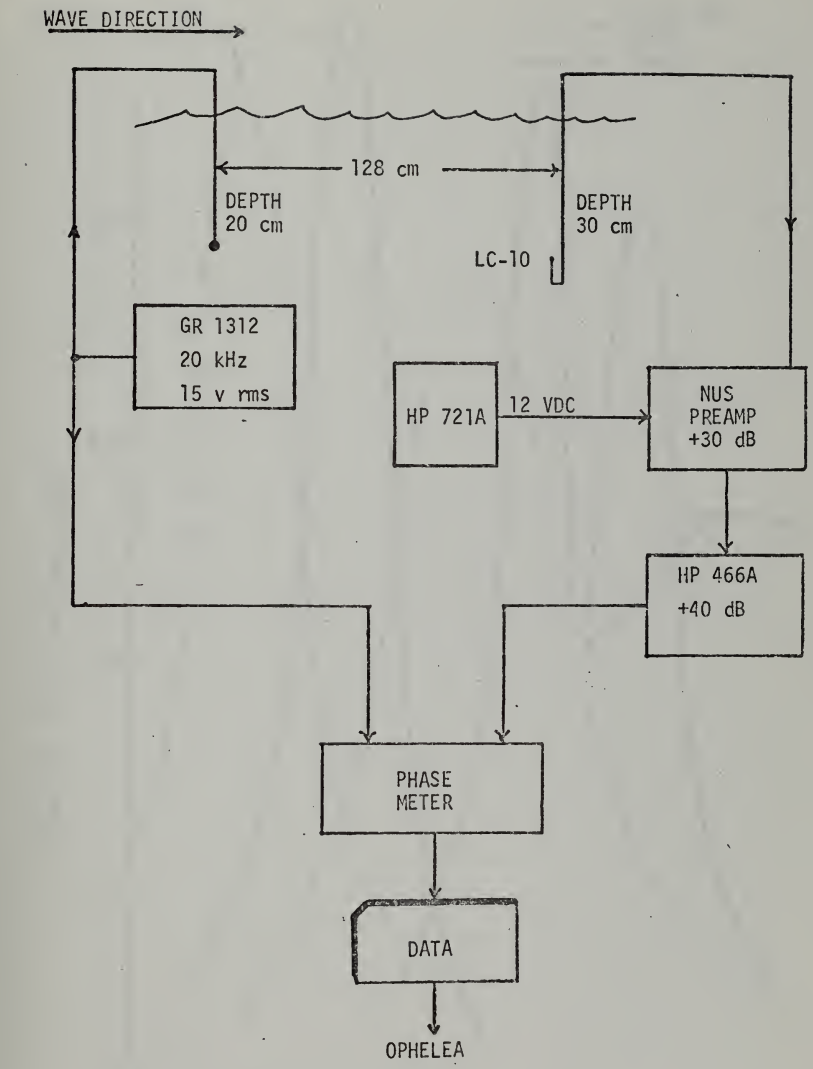

Figure 12. Experimental Setup for Investigating the Phase Characteristics of Scattered Sound

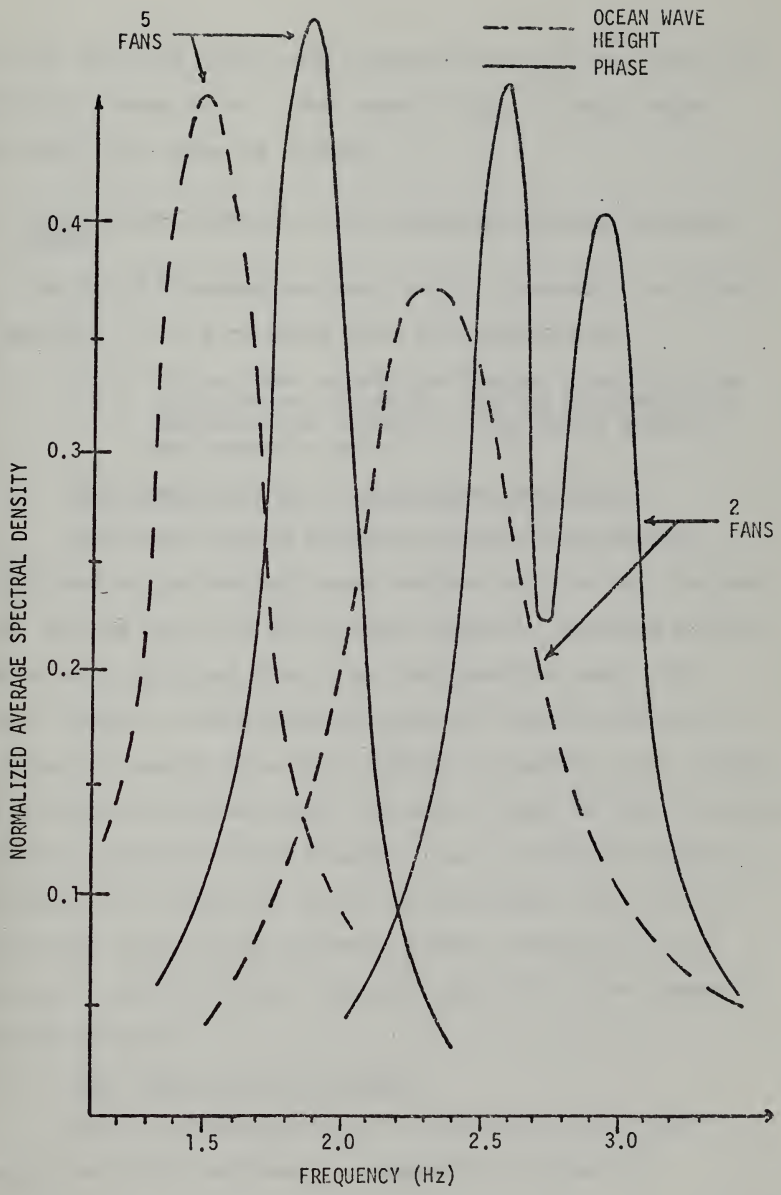

Figure 13. Spectral Density of Phase Fluctuations of Scattered Sound

as well with the ocean wave height spectra as the amplitude modulation spectra do. The cause of the bi-modal shape for the 2 fan curve is unknown.

C. REDUCING FLUCTUATIONS AND INCREASING AVERAGE RECEIVED POWER

The third intermediate goal of this research, as given in Section I.B, is repeated here for convenience:

> iii) investigate signal processing possibilities to decrease, minimize, and/or eliminate the cancellation effects of the ocean surface on acoustic waves

1. The Simple Method — Directional Receivers

The most obvious method to reduce fluctuations introduced by the moving ocean surface is also the simplest. That is, the use of a directional receiver, pointed toward the sound source and away from the ocean surface, will surely reduce fluctuations that result from the reflection of acoustic energy from that surface. However, even though the surface reflected signal varies in time, it still contains acoustic energy from the source. The use of a directional receiver will certainly reduce fluctuations, but it also eliminates much of the acoustic energy available to the receiver. The following reasoning explains a new approach to this dilemma.

2. The Phase-Shift Viewpoint

Due to inhomogeneities in the medium, and time varying boundary surfaces, a transmitted signal of

$$p_s = A \cos \omega t$$

will arrive at a point receiver by way of various paths. Since the signal takes various paths to the point of reception, each component of the signal, in terms of simple ray theory, will arrive with a different amplitude and phase relative to the source signal. That is, each individual ray can be represented as

$$p_i = A_i \cos (\omega t + \phi_i)$$

At any given instant, the point receiver sums all of the rays, and thus receives

$$p_{point} = \sum_{\substack{\text{all} \\ \text{directions}}} A_i \cos (\omega t + \phi_i)$$

The amplitude for any given ray, A_i, is a function of the total distance traveled by that ray. The variations in A_i are approximately constant in time when compared with temporal amplitude variations in p_{point}. The major fluctuations in p_{point} as time passes are a result of the summation of the random-phase sinusoids. If the variation introduced by the random phases of each component could be eliminated, the fluctuations of p_{point} in time would be greatly reduced.

With this in mind, the use of a directional receiver to reduce fluctuations should be reconsidered. The reduction

in fluctuations obtained by aiming the receiver away from the sea surface occurs because those rays with the most random phase shifts are eliminated.

In a limiting case, the receiver would be of such a high directionality that only one incoming ray of acoustic energy would be accepted. All other components, assumed to be randomly phase shifted, would not be received. Fluctuations would be greatly reduced, but this also wastes almost all of the energy present at the location of the receiver. The situation could be improved if two or more components were in phase; they could be added without any cancellation.

Alternatively, if two components were out of phase, with the phase difference known, a phase correction factor could be inserted before the addition of the two rays.

The generalization easily follows. Select one ray as a reference. Measure the phase difference between each remaining ray and the reference ray – then correct all phase shifts, and add all components. Thus, the fluctuations introduced by the summation of randomly-shifted components would be eliminated.

3. An Analog Example

An analog device to accomplish this phase shifting process could take the form shown in Figure 14. The reference signal and the phase shifted signal could be fed into a phase measuring device. The output of the phase measuring device would be a voltage proportional to the phase shift

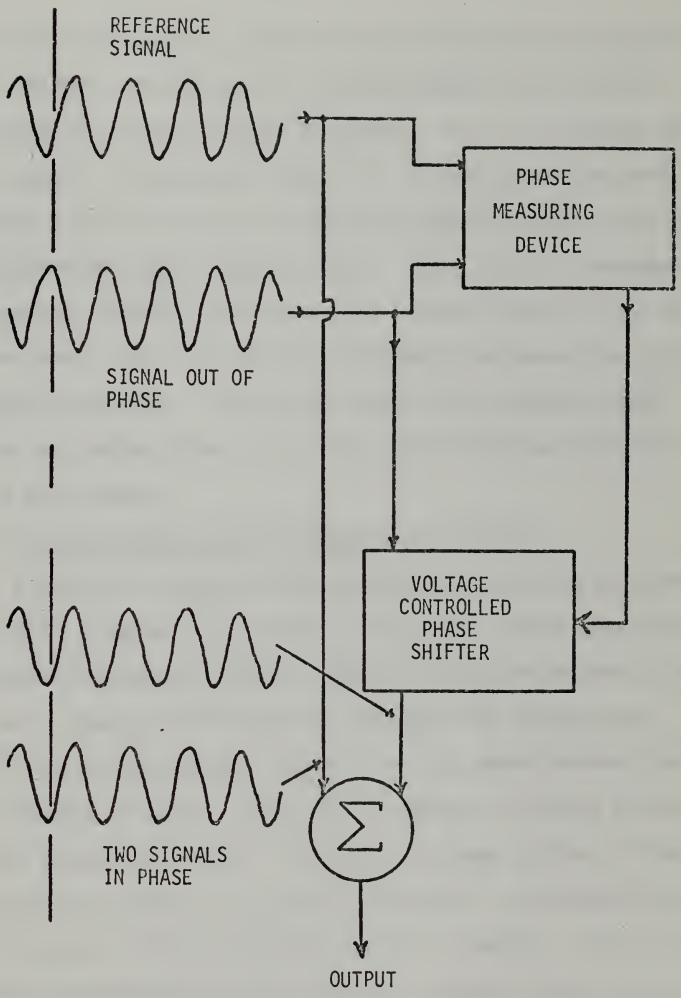

Figure 14. Analog Example of Phase Shift Correction

between the two signals. This voltage would then control a phase shifter, shifting the second signal by an amount which would put both signals in phase. The two signals would then be added. This would result in eliminating fluctuations that would arise if the two original signals with a time varying phase difference were simply added. (The dynamic response of the analog devices is assumed to be much faster than the time span over which the phase difference between the original two signals changes.) Note also that this process would result in an output that would be at its maximum possible value at all times.

4. Digital Phase Shift Correction -- Theory

A digital method of phase shift correction has been used in this research. Consider Figure 15, where two sinusoids of the same frequency, with a phase difference between them, are shown. Equal amplitudes are assumed for simplicity. Suppose both sinusoids are sampled at the same instant for a given length of time. That is, a 'block' of data points from each signal is taken. If each of these blocks of data is processed by means of an FFT algorithm, the results are given in terms of two series of complex numbers. Since pure sinusoids have been assumed, only one complex number in each of the two series will have a non-zero value. Let the complex number representing the first signal be

$$a_1 + jb_1$$

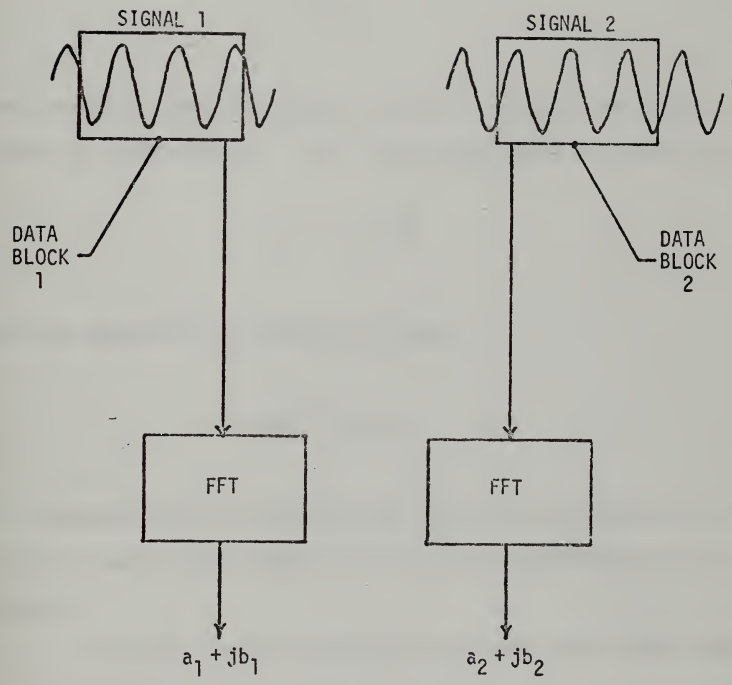

Figure 15. Individual Processing of Two Phase-Shifted Sinusoids

where $j = (-1)^{\frac{1}{2}}$. Correspondingly, let the only non-zero component resulting from the second signal be

$$a_2 + jb_2$$

Each complex number contains certain information about the signal it represents. The signal amplitude is given by

$$(a_i^2 + b_i^2)^{\frac{1}{2}}$$

and the phase of the complex number

$$\tan^{-1} b_i/a_i$$

is a measure of the location of the starting point of the block of data with respect to the zero crossings of the signal.

In most signal processing schemes, the amplitude of the signal

$$(a_i^2 + b_i^2)^{\frac{1}{2}}$$

or the signal power

$$(a_i^2 + b_i^2)$$

is the information of interest. The phase information, to this author's knowledge, is usually discarded or neglected. Here, however, this information can be used to describe the amount of phase shift between the two signals. The magnitude of the phase difference, at the time the data blocks are taken, is given by

$$|\tan^{-1} b_2/a_2 - \tan^{-1} b_1/a_1|$$

An awareness of the fact that this type of phase information is available in the results of the Fast Fourier Transform leads to several interesting signal processing possibilities. Before these possibilities are discussed, first consider what happens if phase shift differences are not eliminated. Two sinusoids are shown again in Figure 16. If a hydrophone receives these two signals with no consideration of the phase difference between them, the data blocks are effectively added. The FFT of this sum will be a complex number representing the sum of the original rays. The power can then be computed as shown on the diagram. This power represents the power that would be received by an omnidirectional hydrophone. Any phase shift between the two original signals has the effect of lowering the output power, even though the total available energy in the field remains constant. If the phase difference varies in time, the voltage and power output will fluctuate. Thus, the technique of adding the data blocks

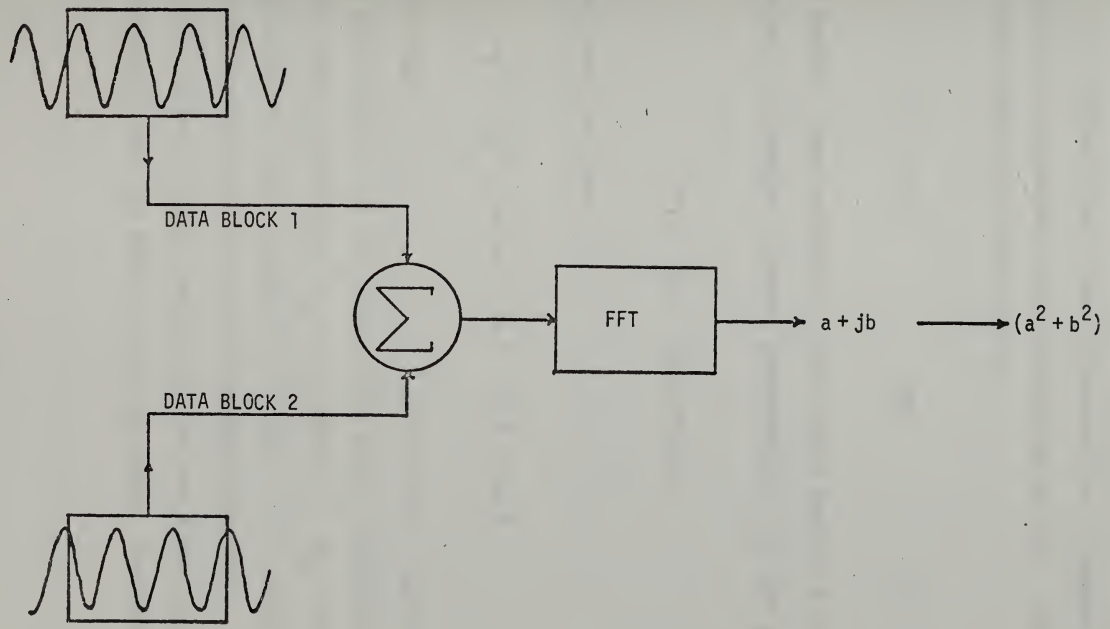

Figure 16. Processing the Sum of Two Phase-Shifted Sinusoids (One Way of Simulating an Omnidirection Receiver)

together before processing simulates the use of an omnidirectional receiver.

Consider now, some alternatives. Suppose the data blocks are processed individually by an FFT. The results of the individual FFTs will be

$$a_1 + jb_1 \qquad \text{and} \qquad a_2 + jb_2.$$

As before, some measure of the signal power is desired. Adding the complex numbers representing the two signals gives

$$(a_1 + a_2) + j(b_1 + b_2)$$

The power is then

$$a_1^2 + a_2^2 + 2a_1a_2 + b_1^2 + b_2^2 + 2b_1b_2$$

Note that a_1, a_2, b_1, and b_2 can be either positive or negative. In particular, for two signals of equal amplitude with a 180° phase difference, $a_1 = -a_2$ and $b_1 = -b_2$, and the power given by the above equation is zero. This process is another way of simulating the omnidirectional receiver. It is equivalent to first adding the signals in the time domain and then processing with an FFT to find the power, as shown in Figure 16.

The crossterms in the above equation will cause the power to fluctuate if the phase difference between the two signals varies in time. One way of reducing the fluctuations is to omit the crossterms. This is exactly what is done if the power of each signal is computed, and the two powers added, as shown in Figure 17. Thus, the Power Sum (PSWSUM) is defined:

$$PSWSUM = (a_1^2 + b_1^2) + (a_2^2 + b_2^2)$$

Suppose now that the absolute values of the a's and the b's are used in the addition of the two complex numbers, and the power then computed. For reasons that will become obvious later, this process has been named the Rotated Vector Sum (RVSUM).

$$RVSUM = (|a_1|+|a_2|)^2+(|b_1|+|b_2|)^2 = a_1^2 + a_2^2 + 2|a_1||a_2| + b_1^2 + b_2^2 + 2|b_1||b_2|$$

The final method of power computation shown in Figure 17, the Magnitude Sum, is obtained by computing the voltage of each signal, adding these voltages, and then squaring to obtain the power. That is,

$$MAGSUM = \{(a_1^2+b_1^2)^{\frac{1}{2}} + (a_2^2+b_2^2)^{\frac{1}{2}}\}^2$$

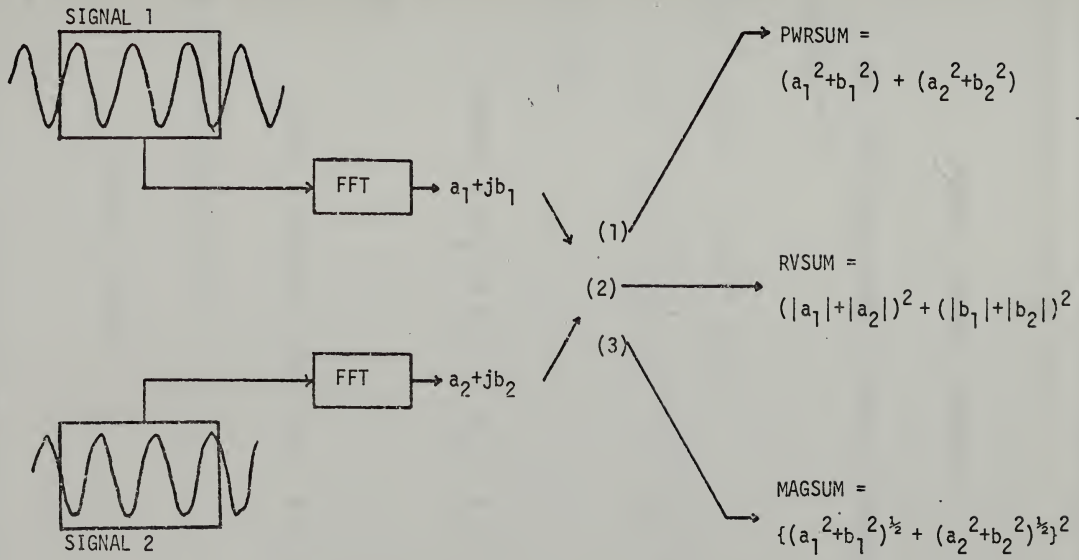

Figure 17. Three Proposed Methods of Processing Individual Sinusoids

The relative sizes of these three quantities, as demonstrated in the discussion to follow, are[1]

$$\text{MAGSUM} \geq \text{RVSUM} \geq \text{PWRSUM}$$

The fact that RVSUM $\geq$ PWRSUM is easily demonstrated. Expanding RVSUM

$$(|a_1| + |a_2|)^2 + (|b_1| + |b_2|) =$$

$$a_1^2 + a_2^2 + 2|a_1||a_2| + b_1^2 + b_2^2 + 2|b_1||b_2|$$

Recall that

$$\text{PWRSUM} = (a_1^2 + b_1^2) + (a_2^2 + b_2^2)$$

Thus,

$$\text{RVSUM} = \text{PWRSUM} + 2|a_1||a_2| + 2|b_1||b_2|$$

From this it follows that

$$\text{RVSUM} \geq \text{PWRSUM}$$

---

[1] A statement concerning the relative size of an 'omni-directional' addition of the two signals cannot be made without assuming some value of phase difference between the two signals.

the equality holding only when a_1 or a_2 and b_1 or b_2 equal zero.

To demonstrate the fact that the Magnitude Sum is always greater than or equal to the Rotated Vector Sum, the triangle inequality [Ref. 14] is used. That is, for any two complex numbers z_1 and z_2,

$$|z_1| + |z_2| \geq |z_1 + z_2|$$

Letting z_1 and z_2 represent the results of the FFT of signal 1 and signal 2 respectively,

$$|a_1 + jb_1| + |a_2 + jb_2| \geq |a_1 + jb_1 + a_2 + jb_2|$$

or

$$(a_1^2+b_1^2)^{\frac{1}{2}} + (a_2^2+b_2^2)^{\frac{1}{2}} \geq \{(a_1+a_2)^2 + (b_1+b_2)^2\}^{\frac{1}{2}}$$

Squaring both sides gives

$$\{(a_1^2+b_1^2)^{\frac{1}{2}} + (a_2^2+b_2^2)^{\frac{1}{2}}\}^2 \geq (a_1+a_2)^2 + (b_1+b_2)^2$$

Since this result holds for all real numbers, it holds for all positive numbers. That is, the same equation can be written with absolute value signs around each 'a' and 'b'. The left hand side of the previous equation remains unchanged

and the result is

$$\{(a_1^2+b_1^2)^{\frac{1}{2}} + (a_2^2+b_2^2)^{\frac{1}{2}}\}^2 \geq (|a_1| + |a_2|)^2 + (|b_1| + |b_2|)^2$$

Or, in terms of the previous definitions,

$$\text{MAGSUM} \geq \text{RVSUM}$$

A further insight into the nature of the relationship between the Rotated Vector Sum and the Magnitude Sum can be gained by treating the results of the individual FFTs as vectors. Figure 18-a shows two vectors, V_1 and V_2, in the (a,jb) complex plane. The Magnitude Sum

$$\{(a_1^2+b_1^2)^{\frac{1}{2}} + (a_2^2+b_2^2)^{\frac{1}{2}}\}^2$$

simply adds the lengths (or magnitudes, hence the name Magnitude Sum) of the two vectors, and squares the sum. The result is thus independent of the phase difference between the two vectors. Now consider the process defined as the Rotated Vector Sum. As previously stated, this process begins by adding the magnitudes of the real parts and the magnitudes of the imaginary parts to form a new complex number,

$$(|a_1| + |a_2|) + j(|b_1| + |b_2|)$$

18-(a)

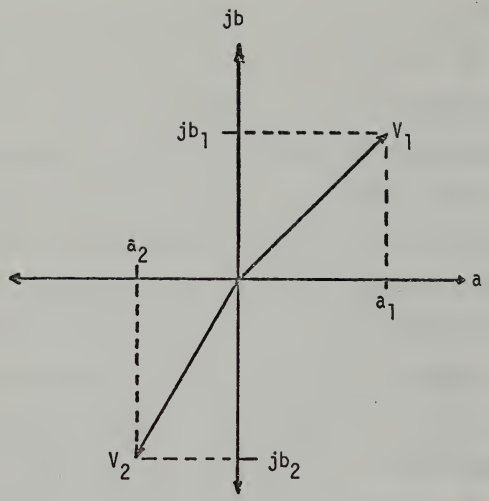

18-(b)

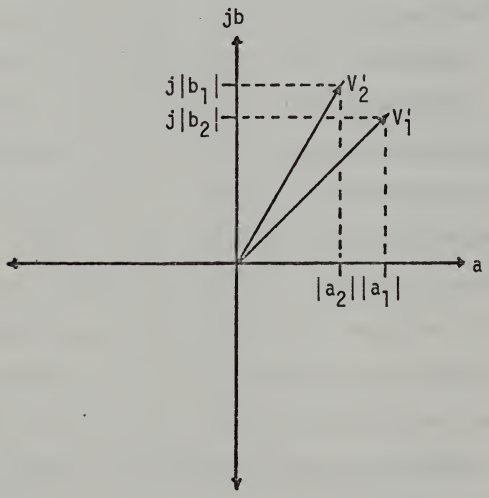

Figure 18. FFTs of Phase Shifted Sinusoids When Viewed as Vectors

The process of using the absolute values is equivalent to rotating both vectors into the first quadrant, as shown by vectors V_1' and V_2' in Figure 18-b. The new complex number formed represents the vector addition of the rotated vectors (hence the name Rotated Vector Sum). Since both vectors are rotated into the first quadrant before the addition, the maximum phase difference that can occur between them is 90°. A measure of the received power is then obtained by taking the square of the magnitude of the complex number representing the sum of the two vectors. Note that it is the use of the absolute value signs in the definition of RVSUM that limits the phase difference between the two signals. If the absolute value signs are not used, no phase correction is introduced; the results are the same as those that would be found in the case of an omnidirectional receiver.

Now that these ideas have been presented, two facts must be re-emphasized so that the experiments described in the following section can be clearly understood and correctly interpreted. First of all, the quantities discussed in this section, MAGSUM, RVSUM, AND PWRSUM, have the dimensions of power. Secondly, the material of this section is highly conceptual in nature. It has been presented only to serve as an elementary model for the experiments that are to follow.

5. Phase Shift Processing of Scattered Sound

The theory of Section IV.C.4 describes several methods to digitally eliminate the constant phase difference between

two perfect sinusoids. The actual situation of interest, the fluctuation of underwater sound scattered from the sea surface, is more complicated in three major ways:

1) the elementary model has been proposed in terms of single 'rays' — a bundle of 'rays' would be received by a transducer in the real world

2) the elementary model corrects phase differences that are constant in time — this is certainly not the case for the fluctuating signals of interest here

3) the perfect nature of the theoretical signals used in the model cannot be realized in practice — thus the results of an FFT for a block of data will be a series of complex numbers rather than a single complex number

As stated above, the first drawback in attempting to process scattered sound by phase shift elimination arises from the fact that the simple model is based on ray theory. A 'ray' is merely a concept, it does not exist in the real world. Hence, attempting to design a receiver to detect a ray is an absurdity. But recall the role of directional receivers in reducing fluctuations. The receiver is aimed at the source, eliminating cancellations that arise due to surface reflections. At the same time however, acoustic energy reflected from the surface is eliminated. Why not aim a second receiver at the surface to pick up the reflected signal? This is exactly what is done in the following.

An array was constructed in which two circular, 12.7 cm radius, mylar transducers were used as receivers. The elements were mounted side by side on a rack as shown

in Figure 19. The rack was designed so that both elements could be independently trained in the vertical plane by means of pushrods. Thus, one receiver could be aimed directly at a source, while the other receiver could be adjusted to pick up reflected signals from other directions. (For a time varying ocean surface, these two signals certainly would not be pure sinusoids with a constant phase difference. But they would represent the signals of interest in the acoustic fluctuations case. That is, two signals, generated by the same source, with two different travel paths, would be available at one location for some type of phase shift correction.) Figure 20 shows the amplifiers and filters used for signals picked up by the mylar receivers. The 300 volts dc used to polarize each of the receivers was supplied by a Burgess U-200 B-type battery.

The second problem in extending the elementary model, the temporal variations in the phase difference between the two signals, was solved by means of a computer program designed to 'sample and wait'. That is, the two signals from the array are fed into separate channels of the A/D converter. The computer simultaneously takes a block of data points from each signal, and then writes the information in a 'block' format on a digital cassette. After a specified delay, another block of data is taken from each signal, and the data are again stored. This process continues until a desired number of data blocks have been taken from each

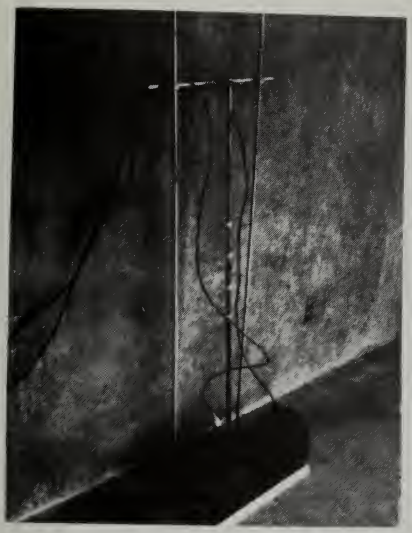

Overall View

Side View

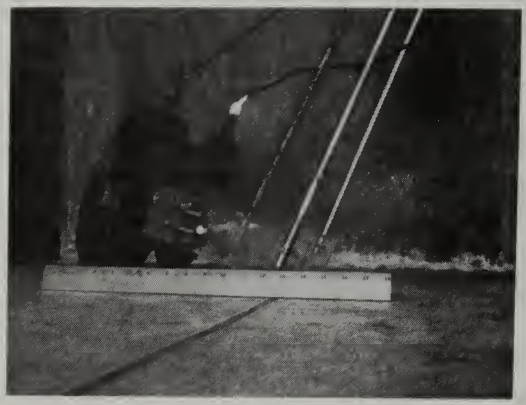

Figure 19. Two-Element Array Constructed Using Two Mylar Transducers

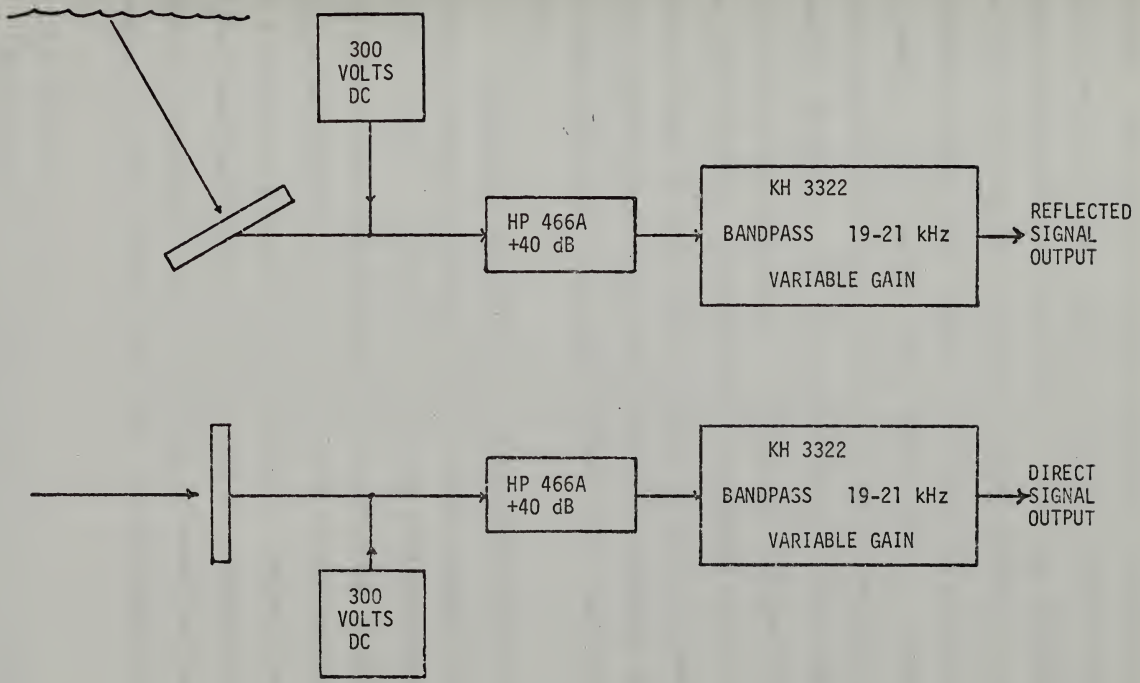

Figure 20. Amplifiers and Filters Used for Signals Received by Mylar Transducers

channel. The program is quite flexible in that the number of points per block, the sampling frequency, and the total number of points can be specified.[1] When the program has finished, all the data blocks have been stored on a digital cassette. Recall from Section IV.B that the temporal changes of phase in the acoustic signal occur slowly. In fact, they occur over the time spans similar to those characteristic of temporal changes in the ocean wave height. Thus with proper selection of the parameters in the sample and wait program, the phase difference between the two signals at the time a block of data is taken will be approximately constant. Proper selection of delay time allows the temporal changes of phase difference to be investigated on a block by block basis.

The third complexity in attempting to phase-shift process fluctuating acoustic sound arises because the elementary model is described in terms of pure sinusoids. For the case of real signals and finite resolution analog to digital conversion, the FFT of a block of data points will be a series of non-zero complex numbers. Hence, the complex number representing the sinusoid must be singled out from the rest of the series. This is done by choosing the complex number with the largest magnitude. If the amplitude of the

---

[1]Since one block is taken from each of two channels at a given instant, the total number of blocks is specified by the total number of points divided by two times the number of points per block.

sinusoid is large compared to any background signals, the largest complex number will represent the signal. The smaller complex numbers represent the frequency content of the low level background disturbances. When this number has been selected, the previously discussed MAGSUM, RVSUM, and PWRSUM can be computed. This technique was used in a second computer program designed to read the blocks of data from the digital cassette, and to process the data in several ways.

To summarize, the basic steps of the experimental procedure are shown in Figure 21. A source-receiver configuration is set up in the OAWF using the two element array (a). The direct and reflected signals are fed into the OPHELEA system where data are gathered by the sample and wait program (b). The output of the sample and wait program is a series of data blocks taken from the direct and reflected signals at evenly spaced intervals (c). This information is stored on digital cassettes and is then available for processing by the OPHELEA system in several ways. Adding two parallel data blocks and then computing the power by means of an FFT (d) replaces the action of an omnidirectional receiver for signals from two directions. The results of this computation are appropriately named PSEUDO-OMNI. Each data block is also FFTd individually, as shown in part (e) of Figure 21. From these results, the power of the direct signal and the reflected signal, and their phase difference can be computed. The individual FFTs also permit calculation of the previously

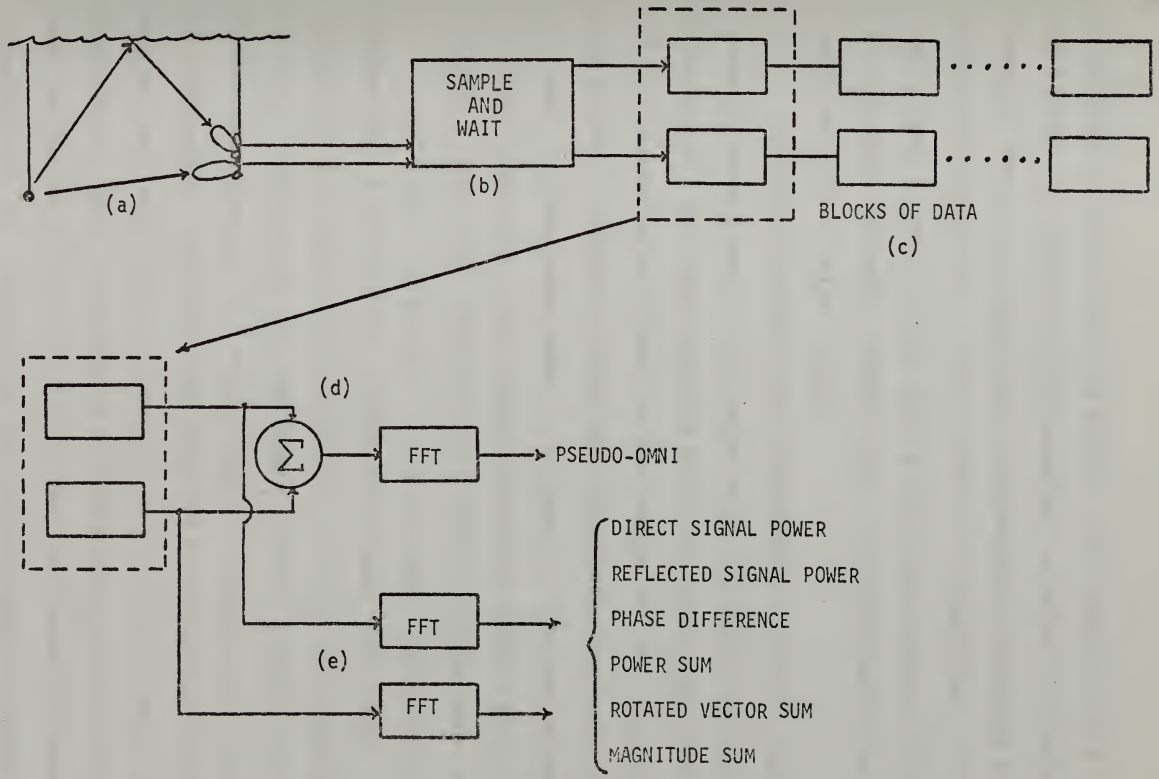

Figure 21. Summary of Basic Experimental Procedure

discussed MAGSUM, RVSUM and PWRSUM. The results for a series of blocks are printed by the computer as shown in Figure 22. Reading down any column shows the temporal dependence of that particular quantity. The time scale is determined by the delay used between blocks during the sample and wait process. The maximum, minimum, average, and a standard deviation of each quantity is also listed.

Before proceeding with experiments involving actual acoustic measurements, the phase shift correction program was tested. The test involved using two equal amplitude 20 kHz sinusoids as inputs to the sample and wait program. The phase difference between the two signals could be controlled by means of the setup shown in Figure 23. The Hewlett-Packard Function Generator with Trigger/Phase-Lock Module puts out a variable amplitude, phase shifted version of the input wave.

The two signals at (a) and (b) are thus identical except for a controllable phase difference. Runs were conducted for phase shifts from zero to 180° in increments of 10°. The results for the MAGSUM, RVSUM, PWRSUM, and PSEUDO-OMNI are plotted versus phase difference in Figure 24. The statement concerning the relative magnitudes of MAGSUM, RVSUM, and PWRSUM made in Section IV.C.4 clearly holds for this case. Note the symmetry of RVSUM about the 90° point, and the rapid fall off of PSEUDO-OMNI for phase differences greater than 90°. Note also that PWRSUM remains constant (the amplitudes of the inputs were held constant throughout the test) but is about 3 db down from MAGSUM.

BLOCK NUMBER	DIRECT POWER	REFLECTED POWER	PHASE DIFFERENCE	PSEUDO-OMNI	PWRSUM	RVSUM	MAGSUM
1	xxx	xxx	xxx	xxx	xxx	xxx	xxx
2	xxx	xxx	xxx	xxx	xxx		
3	xxx	xxx	xxx	xxx			
4	xxx	xxx	xxx				
5	xxx	xxx	xxx				
6	xxx						
.							
.							
.							
.							
MAXIMUM	xxx	xxx	xxx	xxx			
MINIMUM	xxx	xxx	xxx				
AVERAGE	xxx	xxx					
STD. DEV	xxx						

Figure 22. Format of Experimental Output

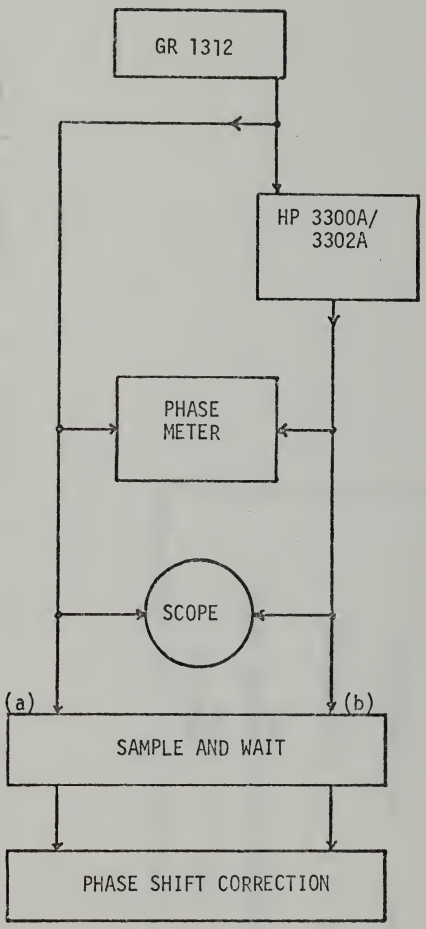

Figure 23. Setup for Testing Phase Shift Correction Processing

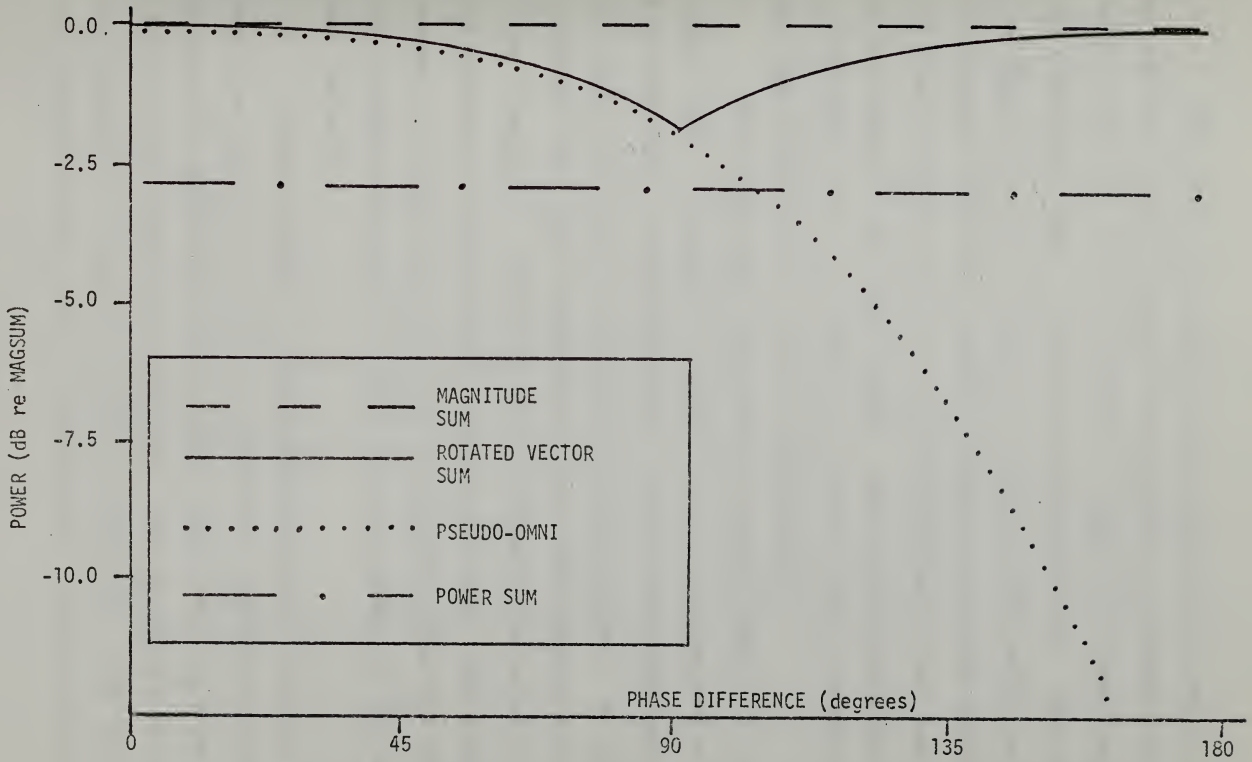

Figure 24. Results of Test of Phase Shift Correction Program

This test indicates that the experimental setup can be used to process phase-shifted laboratory generated sinusoids. For this case, the system is adequately described by the elementary model discussed in Section IV.C.4. This test does not reveal how the system will behave when multi-ray fluctuating underwater acoustic signals are used as inputs, nor does it reveal whether or not the system in that case can be described by the simple model. Some trends have been established, but valid conclusions for the case of scattering can come only from the actual investigation.

Data runs were conducted for several cases. In all cases, OMNI was fixed at a depth of 85 cm, and was driven by a 60 volt (p-p), 20 kHz sine wave. An HP 467A amplifier was used with the GR1312 to provide the source signal. At this frequency, the mylar transducers have a 3-db beamwidth of about 8 degrees. Throughout the experiment, the depth of the receiving array was held constant at 75 cm. The distance between the source and the array (hereafter called the RANGE) was variable, as were the angles of each element in the array. See Figure 25.

It was desired to investigate situations where the array was located at either a Lloyd Mirror maximum or minimum, in order to investigate the extreme cases. To find these locations, the same LC-10 hydrophone used in Section IV.B was mounted on the array as shown in Figure 26. The LC-10 was located in the plane of the receiving elements, and between

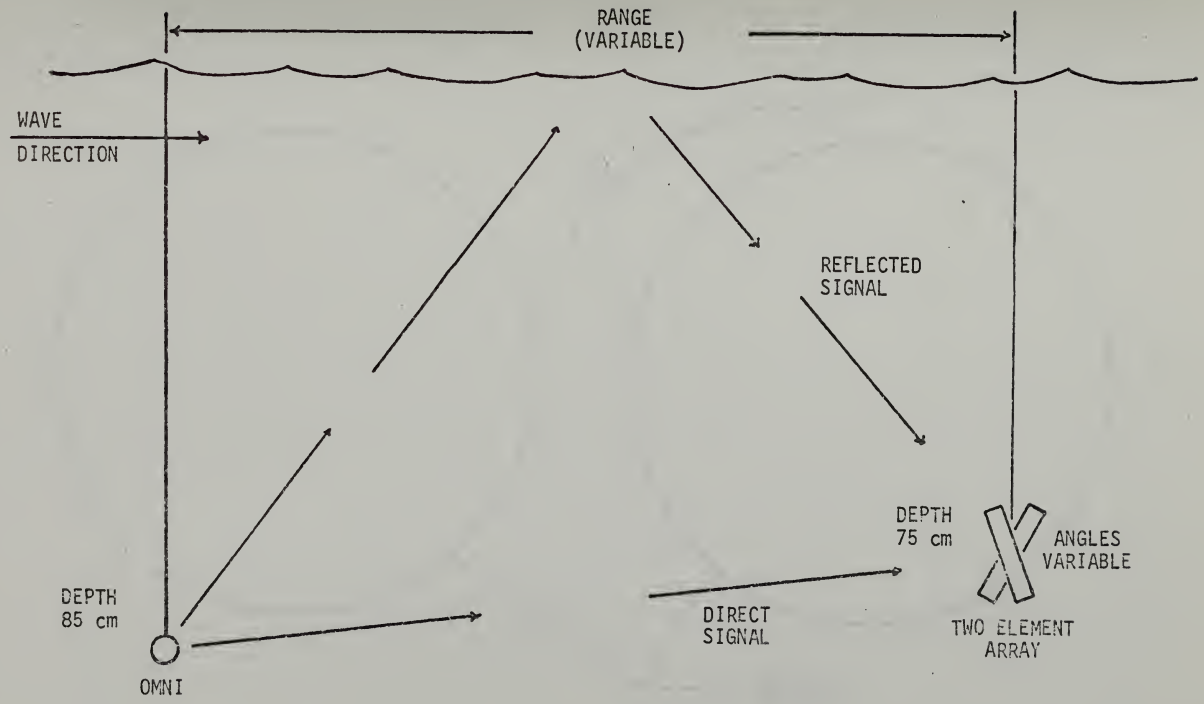

Figure 25. Source/Receiver Geometry for Data Runs

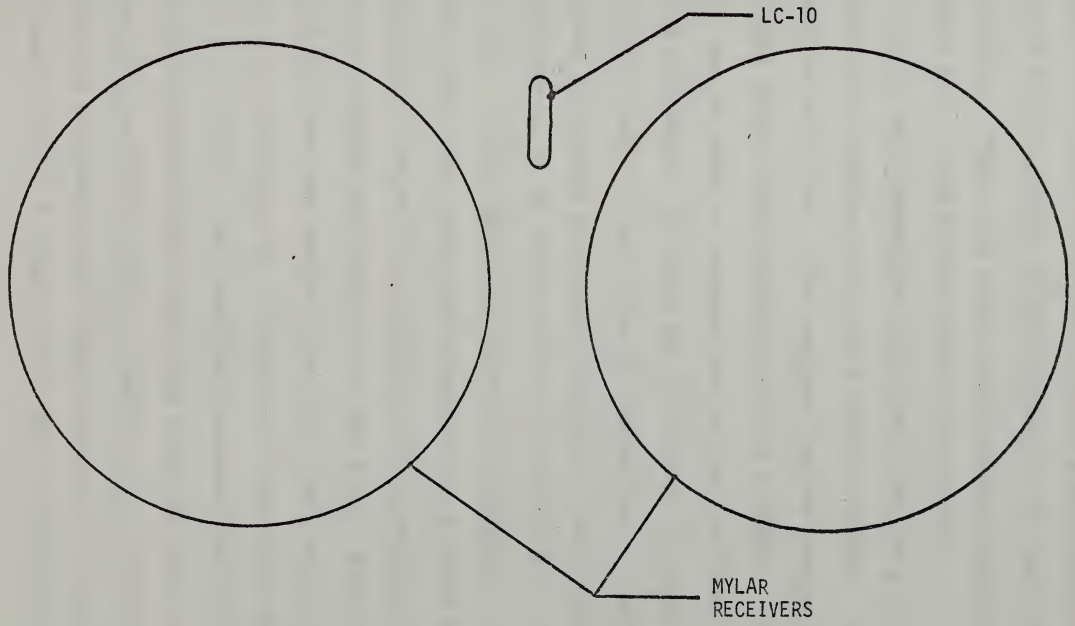

Figure 26. Diagram Showing Location of LC-10 on the Two Element Array

the two receivers. By varying the RANGE (with no fans blowing) the output of the LC-10 was observed to pass through several maxima and minima, which is characteristic of the Lloyd Mirror Effect. Thus, the array could be approximately positioned at a Lloyd Mirror maximum or minimum.

Using this technique (again with the fans off), the array was first located at a Lloyd Mirror maximum. The RANGE was found to be 201 cm. The receiver angles were then adjusted for maximum direct and maximum reflected signals. (The geometry can be used to compute the angles, and thus the roughness parameter, by using the fact that the angle of incidence is equal to the angle of reflection.) Several preliminary runs were conducted to measure noise levels, which were found to be about 30 to 35 db below the usual signal level. Seven data runs were then conducted. After these data runs, the array was relocated to a Lloyd Mirror minimum, again with no fans blowing, and using the LC-10 as a guide. The RANGE was found to be 206.4 cm. After re-adjusting the receiver angles, data runs were again conducted. All data runs consisted of 64 blocks of data, with 64 samples taken in each block. The sampling frequency was 80 kHz, and a simple computation shows that each block of data covered 16 cycles of the 20 kHz signal. Delay time between blocks was varied to increase either the resolution or the time span of the data record. A sample delay time calculation is now given.

From the ocean wave height spectra shown in Section IV.A, the maximum wave height frequency is about 4 Hz. Thus, the minimum ocean period is about .25 seconds. Suppose a resolution of 8 blocks per ocean period is desired. Since 16 cycles of the 20 kHz signal are sampled in one block, the total time for sampling in one ocean period is

$$\frac{8 \text{ blocks}}{\text{ocean period}} \times \frac{16 \text{ cycles}}{\text{block}} \times \frac{1 \text{ sec}}{20{,}000 \text{ cycles}} = \frac{6.4 \text{ msec}}{\text{ocean period}}$$

Since the ocean period is 250 milliseconds long, this leaves 243.6 msec of total delay time. Eight delays are required during one ocean period, so the delay between blocks for this case is 243.6/8 or 30.45 msec. The total length of the data record can be found from

$$\frac{64 \text{ blocks}}{\text{data record}} \times \frac{16 \text{ cycles}}{\text{block}} \times \frac{1 \text{ sec}}{20{,}000 \text{ cycles}}$$

$$+ \frac{63 \text{ delays}}{\text{data record}} \times \frac{30.45 \text{ msec}}{\text{delay}} = \frac{1.969 \text{ sec}}{\text{data record}}$$

A summary of the data runs at the two locations described above is given in the following table:

Run Number	Position	# of Fans	Delay (ms)
1	Max	0	30.45
2,3,4	Max	2	30.45,60.90,91.35
5,6,7	Max	5	30.45,60.90,91.35
8	Min	0	30.45
9,10,11	Min	2	30.45,60.90,91.35
12,13,14	Min	5	30.45,60.90,91.35

The still water runs (no fans) were conducted to obtain undisturbed power levels and phase differences. The results of these two runs indicated that the use of the LC-10 to position the much larger array at a Lloyd Mirror maximum or minimum was not ideal. At a position where there is a true maximum, the signals should be in phase, whereas at a true minimum, the two signals should be 180° out of phase. The computer analysis revealed that the actual phase differences were roughly 45° at the assumed maximum and 71° at the assumed minimum. For all of the above runs, it was found that

MAGSUM > RVSUM > PSEUDO-OMNI > PWRSUM.

Comparison of these trends with Figure 24, which shows the behavior of each processing technique for pure sinusoids with various phase differences, indicates that the processing of the multiple ray acoustic signals is adequately described by the elementary model in this case. The results are shown graphically in Figures 27 and 28. The units of the ordinate are computer generated numbers and are directly proportional to power. The height of each bar represents the average of the three runs at a given position for a given number of fans. For example, runs 2,3, and 4, which were all conducted at an assumed Lloyd Mirror maximum with two fans blowing, were averaged together. The results for each run on an individual basis are presented in Appendix A.

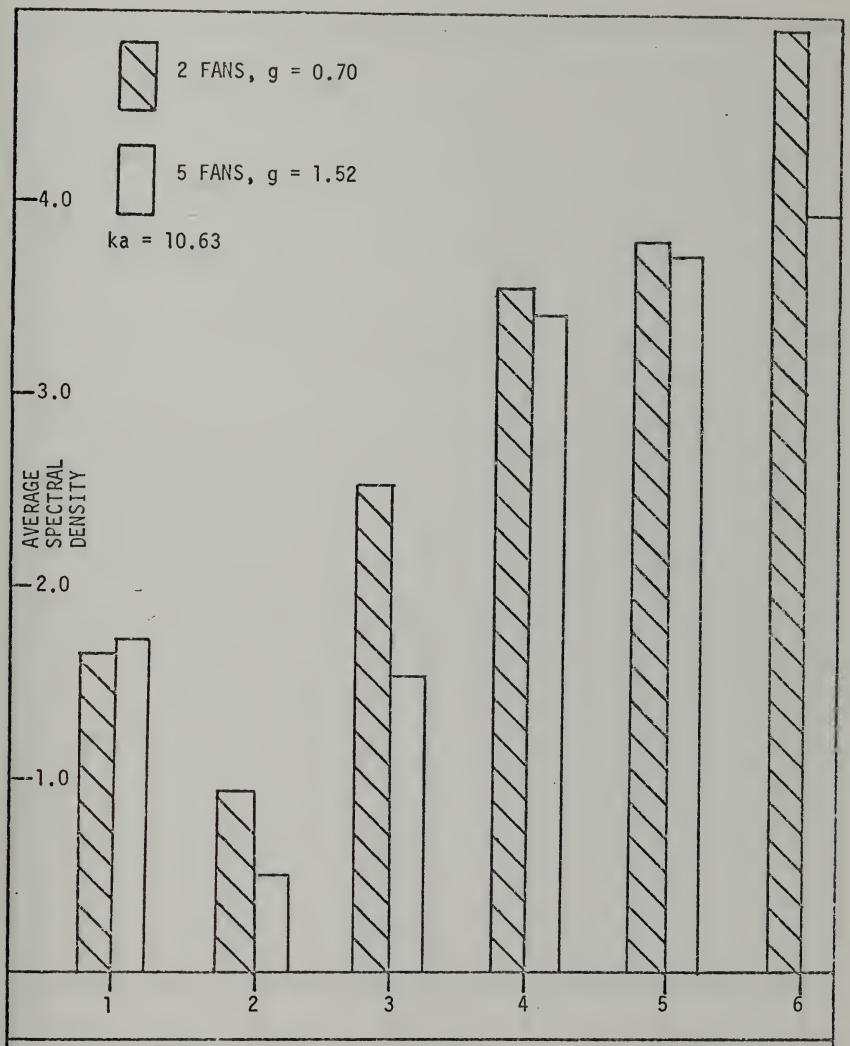

Figure 27. Average Powers at Assumed Lloyd Mirror Maximum

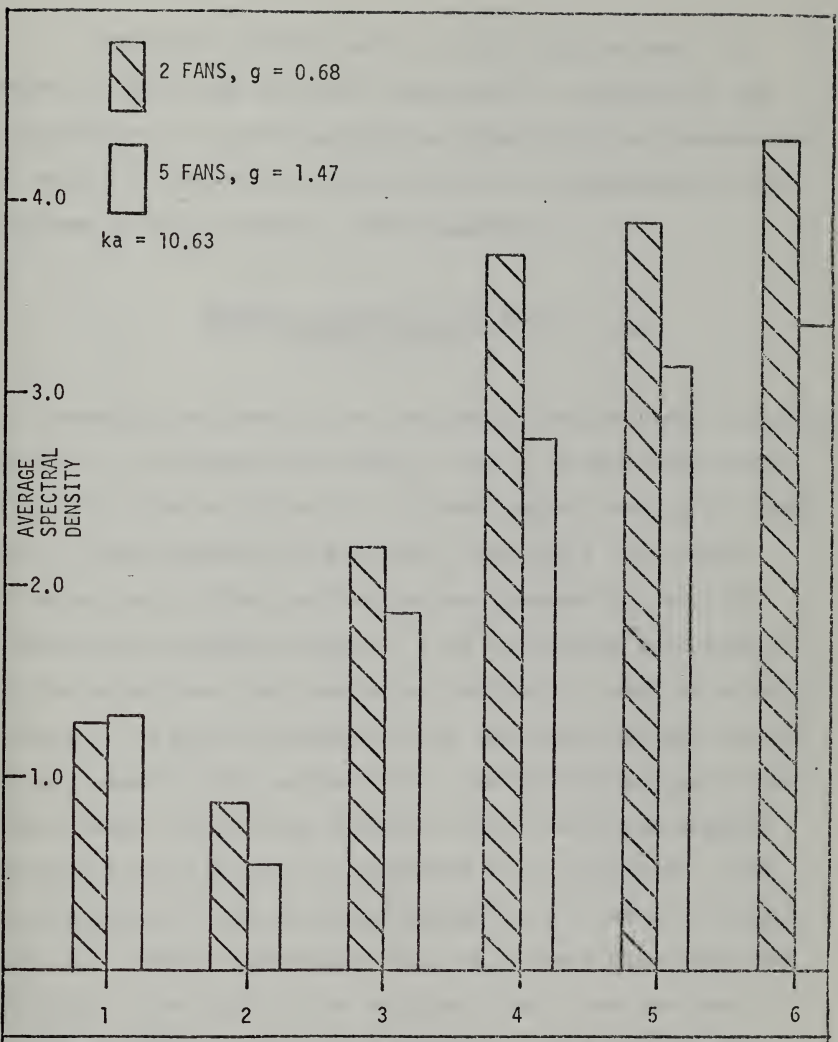

Figure 28. Average Powers at Assumed Lloyd Mirror Minimum

Also of interest here are the fluctuations. In order to make some suitable comparisons, a measure of the fluctuations of each quantity was obtained by expressing the standard deviation of each quantity as a percentage of the average of that quantity. This quantity,

$$\frac{\text{standard deviation of power}}{\text{average power}} \times 100$$

is hereafter referred to as the coefficient of power variation, or CPV. The results for runs 2-7 and 9-14 are shown graphically in Figures 29 and 30. Several points should be noted, all of which pertain to both the 2 fan and 5 fan oceans. First of all, there are fluctuations present in both the direct and reflected signals. This is because each element of the array does not receive an individual 'ray' of acoustic energy. The power fluctuations in the direct signal are low in all cases. They are caused by the orbital motion of the water under the surface, and by surface reflected signals which are received by the sidelobes of the receiver. The fluctuations of the reflected signal in all cases are quite drastic. These fluctuations will be present throughout the analysis -- the only way to minimize them is to use more receivers with narrower beam patterns. Note the relative magnitudes of the CPVs for MAGSUM, RVSUM, PSEUDO-OMNI and PWRSUM. PWRSUM has the least amount of fluctuations, followed

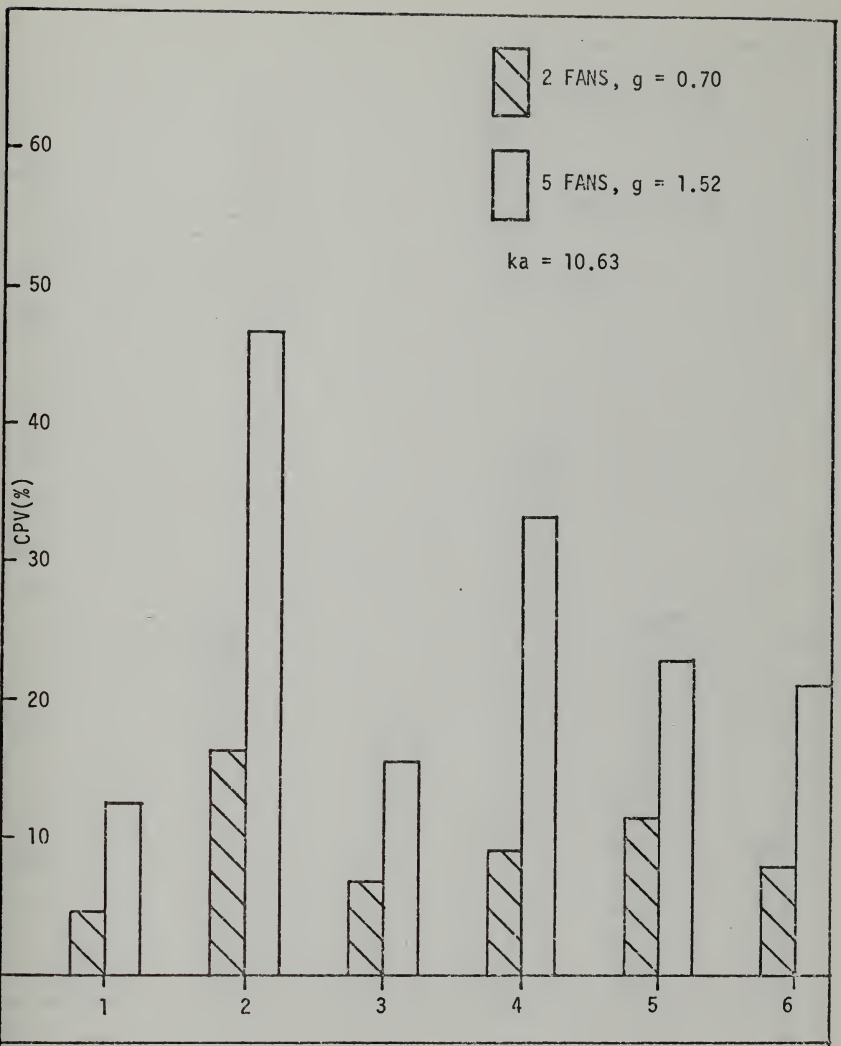

1. DIRECT SIGNAL
2. REFLECTED SIGNAL
3. PWRSUM
4. PSEUDO-OMNI
5. RVSUM
6. MAGSUM

Figure 29. CPVs at Assumed Lloyd Mirror Maximum

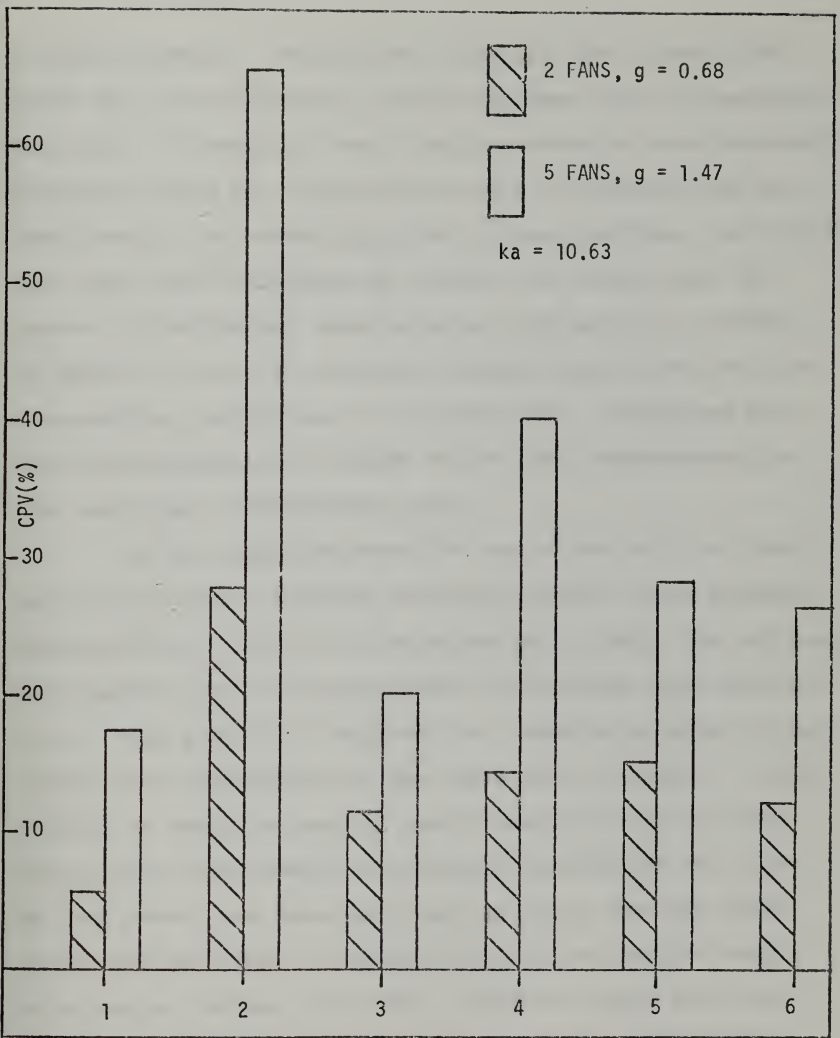

Figure 30. CPVs at Assumed Lloyd Mirror Minimum

closely by MAGSUM. PSEUDO-OMNI displays the highest CPVs, which was to be expected, because no phase shift cancellation was used. In assessing the relative merits of each processing technique, both the fluctuations and the averages must be considered. The PWRSUM displays fluctuations that are slightly less than those displayed by MAGSUM, but recall that the average of PWRSUM was usually about 3 db below the average of MAGSUM. Hence, in terms of average signal power and low fluctuations, as defined by the ratio CPV, it appears that the process defined as MAGSUM is the most advantageous for the case under consideration here.

It was mentioned that the use of the LC-10 to seek out a Lloyd Mirror maximum or minimum proved to be somewhat unsuccessful. Problems in using the LC-10 technique had been anticiapted, but it was not known how serious these problems were. This simplified approach was hampered by what has been termed the 'integration of the Lloyd Mirror Effect'. Simply stated, in order to achieve high directivity, mylar transducers that were several wavelengths in diameter were used as receivers. But then they were so large that the sound field over the face of the receiver did not consist simply of a single maximum or minimum. Thus the sound field was 'integrated' over the face of the receiver. To clarify this situation, and to indicate to what degree it occurred in this case, an IBM-360 computer analysis based on the Lloyd Mirror Effect was used in conjunction with a 3-dimensional

plot subroutine. The results, shown in Figures 31 and 32, show that the sound field over the piston face at the RANGEs previously used (201 and 206.4 cm) was somewhat complicated. Thus, using the LC-10, which is a 'point' receiver, to locate the positions of the Lloyd Mirror extremes for the mylar array would be very difficult, if not impossible.

Therefore, a second method was used to investigate the case where the phase difference between the direct and reflected signals was 180°. The RANGE was set again to 206.4 cm, the location of the approximate Lloyd Mirror minimum. With the fans off, one element of the array was adjusted for the maximum reflected signal. The second receiver was adjusted for the maximum direct signal, and this amplitude recorded. The second receiver was then tuned off the maximum direction (and away from the surface). A phase meter was used to monitor the phase difference between the direct and reflected signals. When the direct signal was adjusted so that the phase difference between the two signals reached 180°, the direct receiver was locked in place, and the amplitude of the direct signal was adjusted back up to its previously measured maximum value. Thus, the worst case of a Lloyd Mirror minimum, that is, a direct and reflected signal with a 180° phase difference, was simulated. Various preliminary runs were conducted, again with no serious noise difficulties. The following runs then were conducted:

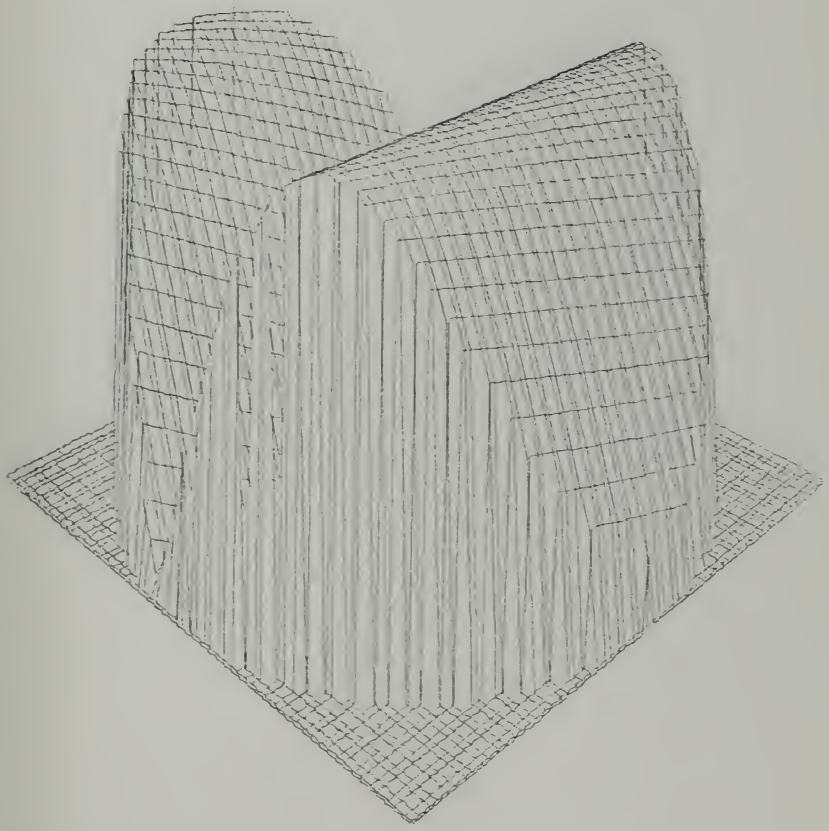

Figure 31. Integration of Lloyd Mirror Effect Over a Piston at Assumed Lloyd Mirror Maximum (ka = 10.63)

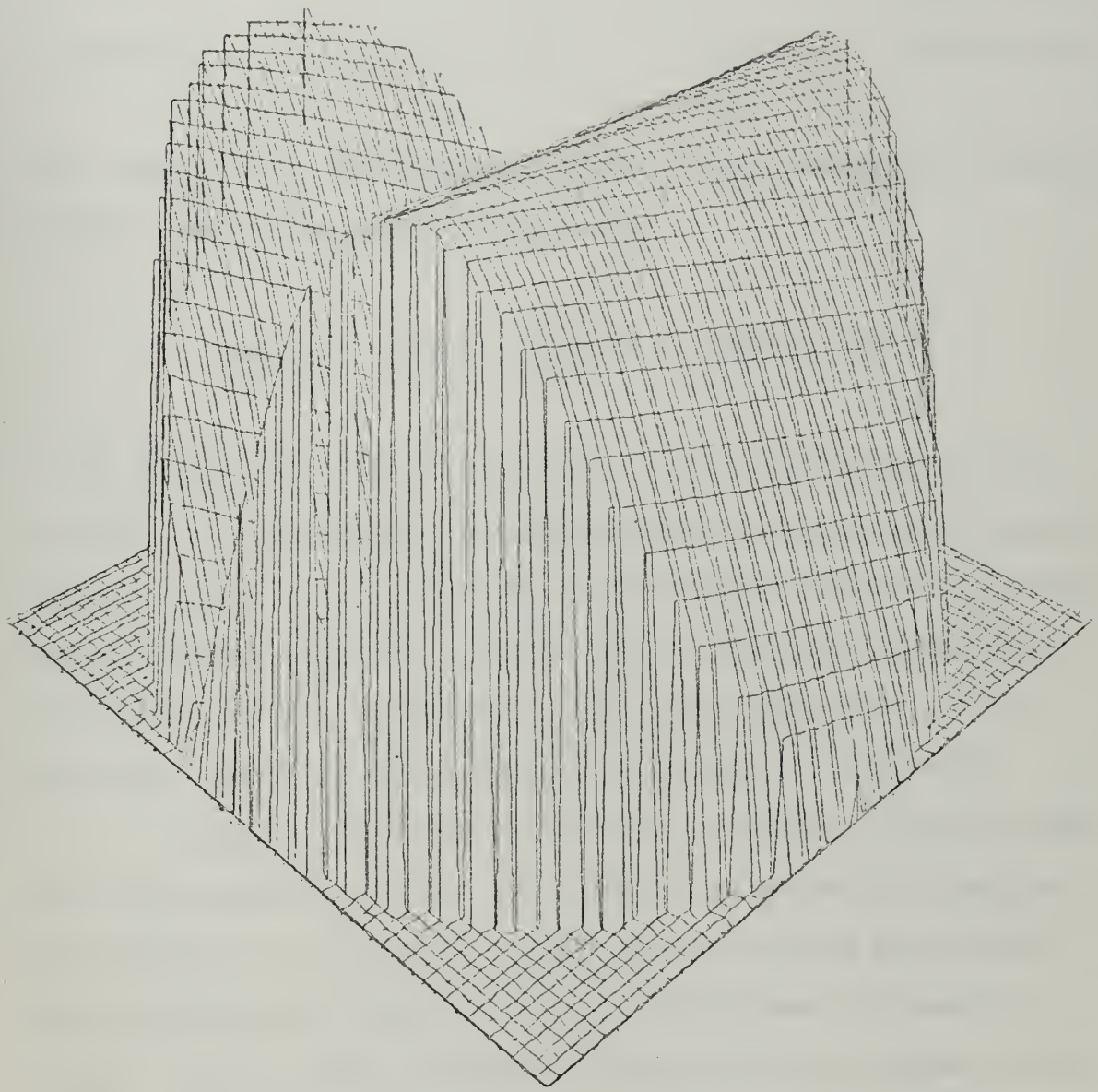

Figure 32. Integration of Lloyd Mirror Effect Over a Piston at Assumed Lloyd Mirror Minimum (ka = 10.63)

Run Number	# of Fans	Delay (msec)
15	0	30.45
16,17,18	2	30.45,60.90,91.35
19,20,21	5	30.45,60.90,91.35

For these runs, the relative sizes of the averages of MAGSUM, RVSUM, PWRSUM and PSEUDO-OMNI were

MAGSUM > RVSUM > PWRSUM > PSEUDO-OMNI

with PSEUDO-OMNI down more than 10 db from MAGSUM in all cases. The low values of PSEUDO-OMNI were expected because of the large still water phase difference between the direct and reflected signals. These trends are again adequately described by the elementary model (see Figure 24). The relative sizes of the averages are shown in Figure 33.

Figure 34 shows the CPVs for these runs as was done for the previous runs at the assumed Lloyd Mirror maximum and minimum. The processes defined by MAGSUM and PWRSUM have reduced the fluctuations in PSEUDO-OMNI by roughly half. As previously stated, however, the fact that PWRSUM is usually about 3 db lower than MAGSUM is a large price to pay for the slight improvement in reducing fluctuations.

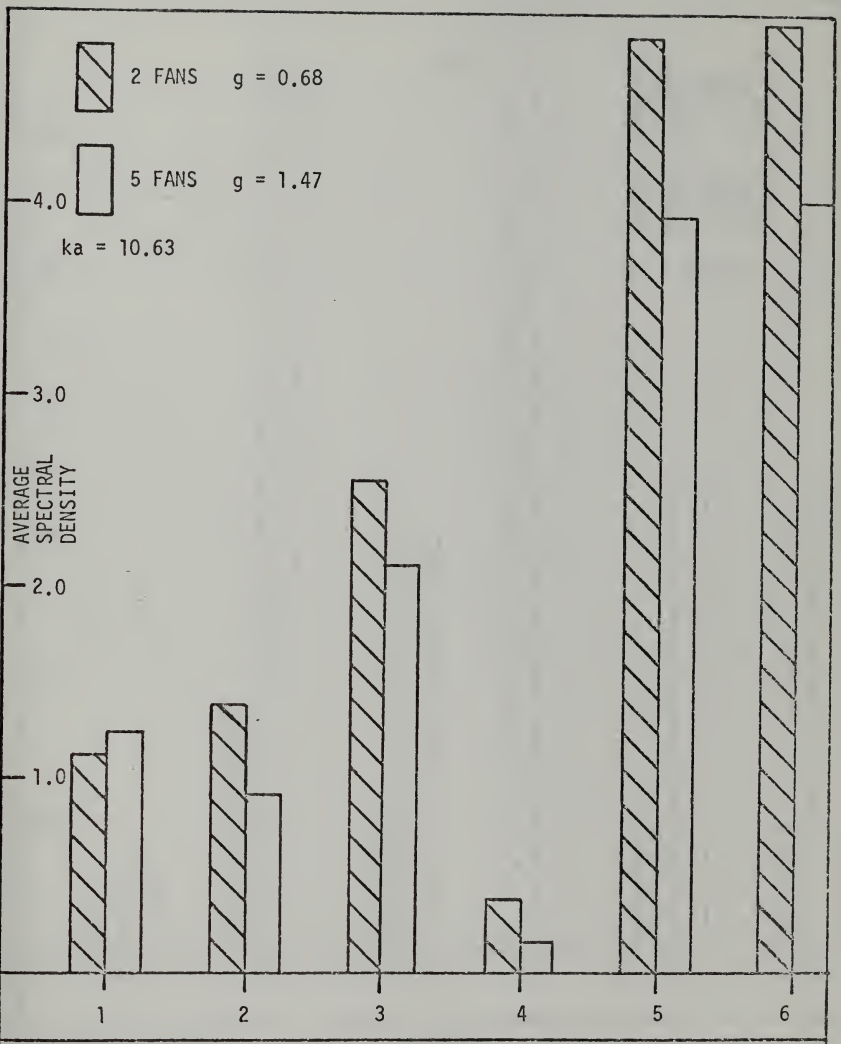

1. DIRECT SIGNAL	3. PWRSUM	5. RVSUM
2. REFLECTED SIGNAL	4. PSEUDO-OMNI	6. MAGSUM

Figure 33. Average Powers at Simulated Lloyd Mirror Minimum

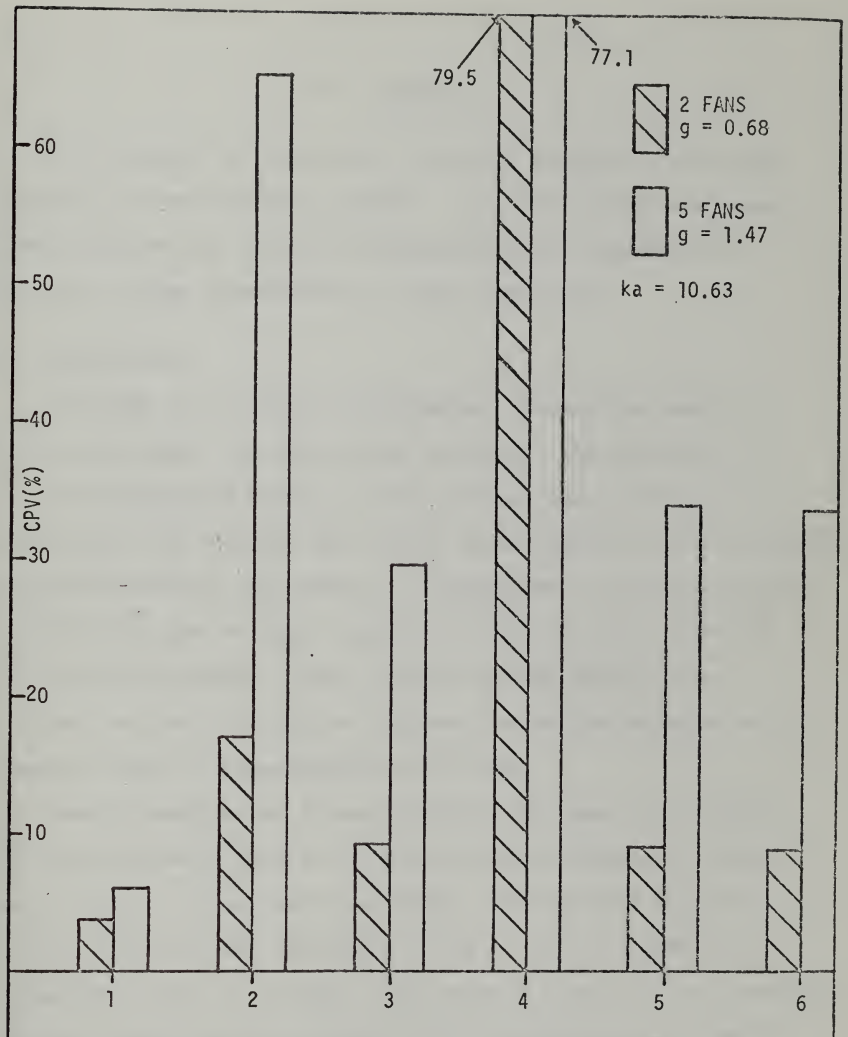

Figure 34. CPVs at Simulated Lloyd Mirror Minimum

V. SUMMARY

This section is intended to briefly summarize the work discussed in the previous pages. Also considered are some possibilities for further investigation and expansion of the basic ideas encountered in this research.

A. CONCLUSIONS

The OAWF at the Naval Postgraduate School was used to accurately model the real ocean surface. The behavior of the wind-generated waves in the tank has been shown to be consistent with results for actual seas found both theoretically and experimentally by others. In addition, the model oceans selected for use in this research affect acoustic waves as predicted by theory. Thus, the use of the model is an accurate and very practical alternative to the expense and complications of experimentation at sea.

Several methods of signal addition by means of digital FFT analysis were used to increase average received signal power and to reduce temporal output fluctuations for two values of acoustical roughness. The theory of phase shift processing gives an insight into certain trends to be expected, and the results of the experimental research seem to follow these trends. Thus it seems that signal enhancement by elimination of phase differences is a practical possibility. At this point, however, the author does not possess enough

information to make definite, quantitative statements concerning the merits of phase shift processing when applied to underwater multipath signals. The idea is new, and it certainly seems useful. A better understanding of the practical applications of the concepts presented in this research will no doubt come with continued experimentation.

B. FUTURE RESEARCH POSSIBILITIES

The main limitation now seems to lie in the design and size specifications of the receivers to be used to pick up the multipath signals. The receivers must be large in order to achieve high directionality, yet they must be small with respect to the acoustic wavelength in order to minimize the previously discussed integration effects over the receiver face. Future research along these lines could procede in two possible directions. First of all, experiments similar to those done in this research could be conducted for receivers of various beamwidths. The relative merits of each signal processing technique could then be investigated as a function of receiver directionality, the goal being to determine trends leading to some optimum receiver size. A second possible method of solving this problem is to use computer analysis as was done to plot Figures 31 and 32 showing the integration of the Lloyd Mirror Effect over the piston face. The parameters of source/receiver depth, range, rms wave height, frequency, etc., could all be used to determine some optimum beamwidth/receiver size relationships.

Future work could also investigate the behavior of the processing techniques as a function of acoustical roughness, g. In this work, roughnesses of approximately 0.7 and 1.5 were used. As mentioned in Section II.A., the statistics of the sound scattered from the sea surface as a function of g are well known. These known statistics could be compared with the statistics of the processing technique which add the direct signal to the scattered signal.

Throughout this research, noise levels were kept as low as possible. Future experiments might investigate the capabilities of the proposed signal processing techniques for signals that are mixed with noise.

The concept of phase shift processing as described in this research is not meant to be the ultimate solution to the difficulties of the multipath propagation of underwater sound. However, it is a new and possibly useful outlook for such problems.

APPENDIX A. RESULTS OF INDIVIDUAL DATA RUNS

Run #	Average Spectral Density x 10^{-8}					
	Direct Signal	Reflected Signal	PSEUDO-OMNI	PWRSUM	RVSUM	MAGSUM
1	1.337	.7834	2.782	2.120	3.476	4.167
2	1.157	.8108	2.631	1.967	3.236	3.899
3	1.786	.9961	4.024	2.752	4.069	5.371
4	1.897	.9925	4.123	2.889	4.208	5.622
5	1.461	.5546	2.823	2.016	3.205	3.781
6	1.907	.4405	2.729	2.347	3.657	4.066
7	1.788	.5119	2.660	2.300	3.610	4.128
8	1.078	.9277	3.424	2.005	3.587	4.006
9	1.043	.8907	3.248	1.934	3.416	3.811
10	1.484	.8736	4.015	2.385	4.220	4.620
11	1.423	.8823	3.056	2.305	4.140	4.536
12	1.438	.4066	2.722	1.895	3.069	3.190
13	1.305	.5693	2.706	1.874	3.245	3.480
14	1.183	.6410	2.850	1.852	3.135	3.473
15	1.113	1.573	.0416	2.687	5.332	5.332
16	1.100	1.258	.0254	2.358	4.692	4.704
17	1.120	1.474	.0612	2.594	5.128	5.148
18	1.112	1.470	.0748	2.583	5.092	5.128
19	1.197	1.026	.2868	2.224	4.200	4.344
20	1.158	.8892	.4964	2.048	3.700	3.875
21	1.145	1.025	.3336	2.170	4.072	4.200

Standard Deviation of Spectral Density x 10^{-8}

Run #	Direct Signal	Reflected Signal	PSEUDO-OMNI	PWRSUM	RVSUM	MAGSUM
1	.0068	.0123	.0270	.0132	.0832	.0250
2	.0621	.1258	.2510	.1487	.5539	.3136
3	.0588	.1467	.3175	.1543	.2908	.3548
4	.0999	.1772	.4181	.2081	.4200	.4620
5	.1583	.2213	.7775	.2858	.6233	.6506
6	.1815	.3106	1.055	.3771	.9019	1.010
7	.2955	.1530	.9054	.3514	.9032	.9276
8	.0260	.0137	.0693	.0383	.2075	.0757
9	.0838	.3542	.5691	.2975	.6368	.6229
10	.0861	.2100	.6165	.2508	.6135	.5555
11	.0590	.1770	.4267	.2047	.5102	.4111
12	.3291	.3076	1.056	.3236	.8066	.8062
13	.1661	.3719	1.264	.4217	1.025	1.054
14	.2030	.3620	1.018	.3847	.8631	.8866
15	.0244	.0392	.0105	.0222	.0393	.0382
16	.0440	.1648	.0236	.1544	.2976	.2964
17	.0381	.3092	.0428	.3100	.5872	.5840
18	.0392	.2588	.0572	.2560	.4376	.4796
19	.0648	.5420	.1928	.5424	1.126	1.170
20	.0840	.6916	.3776	.6768	1.474	1.514
21	.0664	.6756	.2944	.6948	1.469	.2944

BIBLIOGRAPHY

1. Strutt, J.W., Theory of Sound, Dover, New York, 1945.

2. Uretsky, J.L., "The Scattering of Plane Waves from Periodic Surfaces", Annals of Physics, v. 33, p. 400-427, 1965.

3. Meecham, W.C., "Variational Method for the Calculation of the Distribution of Energy Reflected from a Periodic Surface", Journal of Applied Physics, v. 27, p. 361-367, 1956.

4. Heaps, H.S., "Reflection of Plane Waves of Sound from a Sinusoidal Surface", Journal of Applied Physics, v. 28, p. 815-818, 1957.

5. Marsh, H.W., "Exact Solution of Wave Scattering by Irregular Surfaces", The Journal of the Acoustical Society of America, v. 33, p. 330-333, 1961.

6. Marsh, H.W., Schulkin, M. and Kneale, S.G., "Scattering of Underwater Sound by the Sea Surface", The Journal of the Acoustical Society of America, v. 33, p. 334-340, 1961.

7. Meecham, W.C., "On the Use of the Kirchhoff Approximation for the Solution of Reflection Problems", Journal of Rational Mechanical Analysis, v. 5, p. 323-333, 1956.

8. Beckmann, P. and Spizzichino, A., The Scattering of Electromagnetic Waves from Rough Surfaces, The Macmillan Company, 1963.

9. Lysanov, I.P., "Theory of the Scattering of Waves at Periodically Uneven Surfaces", Soviet Physics: Acoustics, v. 4, p. 1-10, 1958.

10. Fortuin, L., "Survey of Literature on Reflection and Scattering of Sound Waves at the Sea Surface", The Journal of the Acoustical Society of America, v. 47, p. 1209-1228, 1970.

11. Lastinger, J.L., "Acoustic Characteristics of Woods at High Hydrostatic Pressure", The Journal of the Acoustical Society of America, v. 47, p. 285-289, 1970.

12. Kinsman, B., Windwaves, Prentice Hall, 1965.

13. Parkins, B.E., "Scattering From the Time Varying Surface of the Ocean", The Journal of the Acoustical Society of America, v. 42, p. 1262-1267, 1967.

14. Kreyszig, E., Advanced Engineering Mathematics, Wiley, 1965.

INITIAL DISTRIBUTION LIST

		No. Copies
1.	Defense Documentation Center Cameron Station Alexandria, Va. 22314	2
2.	Library, Code 0210 Naval Postgraduate School Monterey, Ca. 93940	2
3.	Manager Anti-Submarine Warfare Systems Project Office Attn: ASW -01 Department of the Navy Washington, D.C. 20360	1
4.	Manager Anti-Submarine Warfare Systems Project Office Attn: ASW -12 Department of the Navy Washington, D.C. 20360	2
5.	Commander Naval Electronics Systems Command Attn: PME -124 Naval Electronics Systems Command Headquarters Washington, D.C. 20360	1
6.	Commander, Naval Sea Systems Command Attn: Code (068H1) Mr. C. Smith, Mr. A. Franceschetti Washington, D.C. 20362	2
7.	Director of Acoustic Programs (Code 468) Office of Naval Research 800 N. Quincy Street Attn: Dr. H. Bezdek Arlington, Va. 22219	1
8.	Commander Naval Air Development Center Attn: J. Kacergis, Special Projects Group Warminster, Pa. 18974	1
9.	Professor H. Medwin (Code 61 Md) Physics Department Naval Postgraduate School Monterey, Ca. 93940	5

10. CDR Ned Mayo — 1
Commanding Officer
USS Glover (AGDE-1)
c/o F.P.O.
New York, N.Y. 09501

11. Dr. Jack Harris, Vice President — 1
Pinkerton Computer Consultants Inc.
65 West Street Road
Warminster, Pa. 18974

12. Mr. Tom Lee, Vice President — 1
Pinkerton Computer Consultants Inc.
65 West Street Road
Warminster, Pa. 18974

13. Mr. William Smith — 1
Department of Physics
Naval Postgraduate School
Monterey, Ca. 93940

14. LCDR J.B. Perkins III — 1
Armed Forces Staff College
Norfolk, Va. 23511

15. ENS M.A. Tourville III — 2
117 Buehner Drive
Pittsburgh, Pa. 15237

16. LCDR Dennis Leeth Zveare (Code 212) — 1
Office of Naval Research
800 N. Quincy Street
Arlington, Va. 22219

17. Professor G. Sackman — 1
Electrical Engineering Department
Naval Postgraduate School
Monterey, Ca. 93940

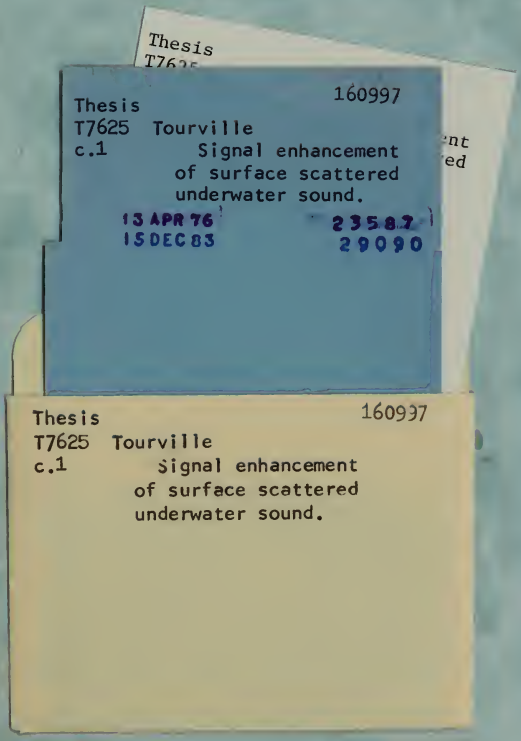
Thesis
T7625
160997
Thesis
T7625 Tourville
c.1 Signal enhancement
of surface scattered
underwater sound.
13 APR 76
15 DEC 83
23587
29090
Thesis
T7625 Tourville
c.1 Signal enhancement
of surface scattered
underwater sound.
160997